J. Phys. Chem. A
January 3, 2011

Theoretical Unimolecular Kinetics for $CH_4 + M \rightleftarrows CH_3 + H + M$ in Eight Baths, M = He, Ne, Ar, Kr, H_2, N_2, CO, and CH_4

Ahren W. Jasper and James A. Miller

Combustion Research Facility, Sandia National Laboratories, PO Box 969, Livermore, CA 94551-0969, USA

Abstract

Ensembles of classical trajectories are used to study collisional energy transfer in highly vibrationally excited CH_4 for eight bath gases. Several simplifying assumptions for the CH_4 + M interaction potential energy surface are tested against full dimensional direct dynamics trajectory calculations for M = He, Ne, and H_2. The calculated energy transfer averages are found to be sensitive to the shape of the repulsive wall of the intermolecular potential, with an exponential repulsive wall required for quantitative predictions. For the diatomic baths, the usual "separable pairwise" approximation for the interaction potential is unable to describe the orientation dependence of the interaction potential accurately, and the ambiguity in the resulting parameterizations contributes an additional uncertainty to the predicted energy transfer averages of up to 50%. On the other hand, the energy transfer averages are shown to be insensitive to the level of theory used to describe the intramolecular CH_4 potential, with a computationally efficient semiempirical tight binding potential for hydrocarbons performing equally well as an MP2 potential. The relative collisional energy transfer efficiencies of the eight bath gases are discussed and shown to be a function of temperature. The ensemble-averaged energy transferred in deactivating collisions $<\Delta E_d>$ for each bath is used to parameterize a single-exponential-down model for collisional energy transfer in master equation calculations. The predicted decomposition rate coefficients for CH_4 agree well with available experimental rate coefficients for M = He, Ar, Kr, and CH_4. The effect of vibrational anharmonicity on the predicted rate coefficients is considered briefly.

I. Introduction

Collisions with bath gas molecules play an important role in controlling the rates of unimolecular and chemically activated reactions. In the low-pressure limit of a unimolecular dissociation,[1] the reaction occurs much faster than collisions with the bath gas, so that every activated molecule has enough time to react before being deactivated. The low-pressure unimolecular rate coefficient is therefore proportional to the rate of activating collisions and to the pressure. (This simple picture may be complicated by tunneling reactions below threshold and by long-lived metastable states above threshold.) At intermediate pressures, unimolecular and chemically activated rates are determined by a competition between intermolecular collisional energy transfer and intramolecular forces.

Pressure dependent kinetics may be characterized theoretically using the master equation (ME),[2,3,4] which, in general, describes the time dependence of the microcanonical state populations of the reactants, products, and intermediates. ME calculations require knowledge of the intramolecular potential energy surface (dissociation energies, isomerization barriers, vibrational frequencies, etc.), which may be obtained with known uncertainties from electronic structure calculations. Likewise, the required intramolecular isomerization and capture rate coefficients may be calculated using transition state theory,[5] with well-validated, predictive strategies for treating barrierless reactions, tunneling, etc. In contrast, the models used in ME calculations for describing collisional energy transfer remain highly empirical.

In principle, predictive theoretical models for pressure-dependent kinetics require detailed knowledge of collision rates and efficiencies as a function of the total energy and total angular momentum of the excited complex. In practice, several simplifying assumptions are often made when modeling energy transfer in the context of the ME. One strategy[4] for constructing and solving the ME involves the following assumptions about energy transfer:

1. The dependence on the initial rotational state of the energized complex is neglected.[6,7]
2. The energy transfer function is assumed to be dependent on the amount of energy transferred but independent of the initial and final energies individually.

(3) The probability distribution of energy transferred per deactivating collision is assumed to be exponential,[1] with the activating probability distribution determined from detailed balance. This approximation is called the "single-exponential-down" model.

None of these assumptions is supported by classical trajectory studies of energy transfer. In fact, energy transfer has been shown to be enhanced by rotational[8,9,10,11] and vibrational[8,11,12,13,14] excitation, with biexponential (or, equivalently, long-tail) probability distributions.[8,11,14]

These assumptions arise in part due to a lack of detailed information about the energy transfer function (assumptions 2 and 3) and in part to facilitate the solution of the ME (assumption 1). More sophisticated treatments of the initial energy dependence and of the probability distribution for energy transfer can be readily included in ME calculations, but such treatments are often not needed. Barker and Weston[11] have recently used classical trajectories to parameterize an energy transfer function that includes angular momentum dependence; ME calculations employing such a so-called "two-dimensional" energy transfer function remain rare, however.

Using the present set of assumptions, the single-exponential-down model requires a single parameter α, which can be associated with the average energy transferred in deactivating collisions[1] $<\Delta E_\mathrm{d}>$. This parameter is often further assumed to be a function of temperature and written

$$\alpha(T) = \alpha_{300}(T/300\ \mathrm{K})^n. \tag{1}$$

Almost every ME prediction of unimolecular and chemically-activated rate coefficients to date has used empirically determined or estimated α_{300} and n. Fortunately, the predicted rate coefficients are often not overly sensitive to these parameters, and similar empirically determined values are typically obtained for similar species, with α_{300} = 50–300 cm^{-1} and $n \approx 1$.

Occasionally, however, surprising values of α_{300} and n are required to reproduce experimental data. For example, in a recent study of CH_3Cl decomposition[15] the values of α required to fit the results of a ME calculation empirically to measured decomposition rate coefficients were found to be four times larger than those obtained in a similar study of CH_4. As another example, low-pressure decomposition rate coefficients for water were calculated[16] using the ME approach, and a relatively weak temperature dependence in α (n = 0.4–0.5) was required to fit the experimental data. It is unclear whether these atypical values of α reflect genuinely "unusual" energy transfer dynamics or instead indicate errors in the measured rate coefficients or are compensating for errors in other parts of the calculation. The transferability of empirically determined energy transfer parameters is also uncertain. For example, when the results of ME calculations[17] fit to measured ethane decomposition rate coefficients above 1500 K were extrapolated to lower temperatures, the theoretical rate coefficients were found to overpredict low temperature experimental values. Rate coefficients over the entire temperature range could be fit by decreasing α_{300} from 120 to 45 cm^{-1} and increasing n from 0.9 to 1.4.[18]

A strategy for obtaining predictive pressure-dependent unimolecular kinetics is clearly desirable. In the context of the ME and assumptions 1–3 outlined above, such a strategy requires a method for predicting $\alpha(T)$. We recently reported[10] the results of ME calculations of rate coefficients for the $CH_4 \rightleftarrows CH_3 + H$ reaction in He using the energy transfer model discussed above, with the parameters α_{300} and n calculated by direct classical trajectories. Errors in the predicted energy transfer dynamics were minimized by using an ab initio potential energy surface and by selecting the trajectories' initial conditions and ensemble averages to be consistent with the ME model. The resulting parameter-free kinetics predictions were shown to be in good agreement with measured rate coefficients.

Here we extend our previous study of CH_4 decomposition in He[10] to include heavier atomic baths (Ne, Ar, and Kr), three diatomic baths (H_2, N_2, and CO), and one polyatomic bath (CH_4). The main goal of this work is to predict $\alpha(T)$ theoretically for these baths using classical trajectories.

As mentioned above, numerous classical trajectory studies of energy transfer have been carried out, and these studies typically invalidate assumptions 1–3. Despite the demonstrated invalidity of these approximations, ME calculations employing these assumptions have nonetheless been used to successfully model a wide variety of unimolecular and chemically activated reactions. It may be that the empirically determined values for α compensate for errors in the energy transfer model. Alternatively, it is possible that the assumptions outlined above, while not physically motivated, do not introduce significant errors into the resulting predicted rate coefficients for some reactions. If fact, several energy transfer models were previously tested for CH_4 dissociation,[7] where it was shown that assumptions 2 and 3 had negligible effects on the predicted kinetics. This result is likely true for any simple dissociation reaction (i.e., for any reaction with one only molecular complex and one set of products). Finally, the results of the classical trajectory dynamics themselves can be uncertain due to the approximate potential energy surfaces and initial conditions employed. Another major goal of the present work is therefore to quantify the errors associated with the classical trajectory calculations, with a particular emphasis on how the description of the potential energy surface affects the computed energy transfer averages. The results of direct dynamics trajectory ensembles are reported here for four baths: He, Ne, H_2, and CH_4. These results are used to test the accuracy of simpler, more efficient analytic and semiempircal descriptions of the potential energy surface. Specifically, the accuracy of representing of the interaction potential as separable from the intramolecular CH_4 potential energy surface and as a sum of fitted pairwise interactions is tested. This separable pairwise approximation is almost always employed in energy transfer studies using classical trajectories.

Classical trajectories have been used previously to study trends in collisional energy transfer efficiencies with respect to the bath gas.[14,19,20,21] In these studies, He has generally been found to be the most efficient atomic collider in contrast to some experimental work.[22,23] Gilbert[19] carefully considered several sources of error in the trajectory calculations for M = He, and the discrepancy between the experimental and trajectory results was ultimately attributed to approximations in the interaction potential energy surfaces used in the trajectory calculations. Gilbert's analysis further motivates the present tests of approximations for the interaction potential typically used in trajectory studies.

Finally, the present predicted values for $\alpha(T)$ for eight bath gases are used in parameter-free ME calculations for $CH_4 + M \rightleftarrows CH_3 + H + M$. The relative efficiencies of the bath gases are discussed, and the predicted decomposition rate coefficients are compared with available experimental rate coefficients for M = He, Ar, Kr, and CH_4. The low-pressure experimental data for Ar and Kr, in particular, provide a more direct test of the energy transfer models and parameterizations than the falloff data previously considered[10] for M = He.

In Sec. II, the present implementation and solution of the ME is briefly discussed, and the direct dynamics and separable pairwise trajectory calculations are described in detail. In Sec. III, validation studies of the approximate potential energy surfaces are presented, a comparison of the predicted bath gas efficiencies is made, and decomposition rate coefficients for CH_4 in He, Ar, Kr, and CH_4 are compared with experimental ones. Section IV summarizes our conclusions.

II. Theory

II.A. Master equation analysis

The ME formalism employed here has been described in detail elsewhere.[4,7] Briefly, for an irreversible unimolecular reaction, the ME governing the microcanonical population densities $n(E,J)$ of the reactant complex (CH_4 in the present work) is

$$\begin{aligned}\dot{n}(E,J,t) = &\sum_{J'}\int_0^\infty dE'\,R(E,J;E',J')n(E',J',t)n_\mathrm{M} \\ &-\sum_{J'}\int_0^\infty dE'\,R(E',J';E,J)n(E,J,t)n_\mathrm{M} - k(E,J)n(E,J,t)\end{aligned} \tag{2}$$

where E and J are the total energy and angular momentum characterizing the energy "grain"[1] or "state" (E,J), $R(E,J;E',J')$ is the 2nd-order collisional energy transfer rate coefficient for a transition from the state (E',J') to another state (E,J), $k(E,J)$ is the microcanonical dissociation rate, and n_M is the concentration of the bath gas. Note that R is implicitly a function of the temperature T and of the identity of the bath gas.

The energy transfer rate coefficient is often written as the product of a total collision rate coefficient

$$Z(E',J') \equiv \sum_{J}\int_0^\infty dE\,R(E,J;E',J') \tag{3}$$

and an energy transfer probability

$$P(E,J;E',J') \equiv R(E,J;E',J')/Z(E',J'), \tag{4}$$

such that P is normalized when integrating and summing over final states (E,J).

At low and intermediate pressures, the solution of the two-dimensional (E,J) ME in eq 2 requires the detailed energy transfer function $R(E,J;E',J')$. Knowledge of the dependence of R on E, J, E' and J' is typically not available. Furthermore, it can be difficult, in general, to enforce the detailed balance condition

$$R(E',J';E,J)g(E,J) = R(E,J;E',J')g(E',J'), \tag{5}$$

where $g(E,J)$ is the thermally equilibrated population of the state (E,J), while including the rotational dependence of R. To facilitate the solution of the ME, we assume that the energy transfer rate coefficient is independent of the initial rotational state[6,7] (assumption 1 from the Introduction), i.e.,

$$R(E,J;E',J') = R(E;E')\varphi(E,J). \tag{6}$$

With this substitution, eq 2 becomes

$$\dot{\bar{n}}(E,t) = \int_0^\infty dE'\,R(E;E')\bar{n}(E',t)n_{\mathrm{M}} - \int_0^\infty dE'\,R(E';E)\bar{n}(E,t)n_{\mathrm{M}} - \bar{k}(E)\bar{n}(E,t) \tag{7}$$

if

$$\sum_J \varphi(E,J) = 1, \tag{8}$$

where

$$\bar{n}(E,t) \equiv \sum_J n(E,J,t), \tag{9}$$

$$\bar{k}(E) \equiv \sum_J k(E,J)n(E,J,t)/\bar{n}(E,t). \tag{10}$$

Equation 7 has the form of a one-dimensional ME, except that $\bar{k}$ depends on $n(E,J)$, which in turn requires the full solution to the two-dimensional ME. Equation 10 can be written[4]

$$\bar{k}(E) = \sum_J k(E,J)y(E,J) / \sum_J y(E,J) \tag{11}$$

with

$$y(E,J) = \frac{\varphi(E,J)}{Z(E,J) + k(E,J) - k_{T,p}}. \tag{12}$$

Assuming $k_{T,p}$ is small and can be neglected when evaluating eq 12 decouples the calculation of $\bar{k}$ from the solution of eq 7.[6,7]

Detailed balance is enforced by writing $R(E,E')$ as

$$R(E,E') = Z\,P(E,E'), \tag{13}$$

assuming Z is an energy-independent Lennard-Jones collision rate, and using the exponential down model (assumptions 2 and 3 from the Introduction)

$$P(E,E') = A\exp(-(E'-E)/\alpha) \qquad E < E' \tag{14}$$

and an empirical model[6] for rotational dependence

$$\varphi(E,J) = (2J+1)\rho(E,J)/\rho(E) \tag{15}$$

$$\rho(E) = \sum_J (2J+1)\rho(E,J), \tag{16}$$

where $\rho(E,J)$ is the state density. (Note that for the spherical top CH_4 there is an additional factor of $(2J+1)$ degeneracy due to the quantum number τ. This degeneracy is included in ρ so that the present equations are suitable for the more general case of an asymmetric top.) The parameter A in eq 14 is chosen such that $P(E,E')$ is normalized, with the activating wing of $P(E,E')$ determined from detailed balance

$$P(E',E)g(E) = P(E,E')g(E'). \tag{17}$$

The single remaining parameter α can be shown to be equal to the average energy transferred in deactivating collisions when α is much less than the threshold energy for dissociation (which is typically the case) for the exponential distribution of $\Delta E = |E - E'|$ in eq 14.[1] Note that the average energy in deactivating collisions is a function of the initial energy E' and that this energy dependence has been neglected. When calculating α with classical trajectories, we choose E' to be close to the dissociation threshold, as discussed below. The parameter α is often written as a function of temperature, as in eq 1.

In the high pressure limit, thermal equilibria are maintained, and the solution to the ME can be written

$$\begin{aligned} k_{T,p}^{\infty} &= \sum_J \int_0^\infty dE\, k(E,J)g(E,J) \\ &= \sum_J \int_0^\infty dE\, k(E,J)(2J+1)\rho(E,J)\exp(-E/k_\mathrm{B}T)/Q \end{aligned}, \tag{18}$$

where Q is the partition function for the dissociating molecule

$$Q \equiv \sum_J \int_0^\infty dE (2J+1)\rho(E,J)\exp(-E/k_\mathrm{B}T). \tag{19}$$

Equation 18 is the usual unimolecular transition state theory rate expression. Collisional energy transfer does not appear explicitly in the high-pressure limit rate coefficient expression; instead, collisions are implicitly assumed to be sufficiently fast and energetic to maintain the thermal populations $g(E,J)$ despite the reaction potentially perturbing these equilibria.

The low-pressure limit rate coefficient can be written[1]

$$k^0_{T,p} = \sum_{J'} \int_0^{E_{J'}} dE' \sum_{J} \int_{E_J}^{\infty} dE\, R(E,J;E',J')x(E',J'), \tag{20}$$

where E_J is the rotationally adiabatic threshold energy for the total angular momentum J and $x(E,J)$ are the normalized steady state solutions of the ME, which are approximately proportional to $\rho(E,J)$ at low pressures.[1] The low pressure rate coefficient is determined by collisions promoting the system from some state below threshold to some state above threshold. Clearly, only states with energies within $\sim\alpha$ of the dissociation threshold can contribute to the low pressure unimolecular rate coefficient. This observation justifies the neglect of the dependence of α on E' for simple dissociation reactions and motivates our choice of E' to be close to the dissociation threshold. At falloff pressures, energy transfer over a wider energy range contributes to the dissociation, but the kinetic effect of the dependence of α on E' is mitigated by the approach to the high pressure limit, which is independent of α.

In the present ME calculations for $CH_4 \rightleftarrows CH_3 + H$, the microcanonical dissociation rates $k(E,J)$ were taken from the CH_3 + H direct VRC-TST capture rate calculation of Ref. 24, transformed via the equilibrium constant, which was calculated as the ratio of rigid-rotor, harmonic-oscillator (RRHO) partition functions. The RRHO partition functions were calculated using experimental values[25] for the zero-point inclusive dissociation energy (36168 cm^{-1}), the frequencies of CH_4 (3019, 2917, 1543, and 1306 cm^{-1}), the rotational constant of CH_4 (5.24 cm^{-1}), the frequencies of CH_3 (3161, 3004, 1396, and 606 cm^{-1}), the rotational constants of CH_3 (9.58 and 4.74 cm^{-1}). (A one-dimensional anharmonic correction to the RRHO partition functions for the umbrella mode of CH_3 based on the calculated potential in Ref. 26 was considered; this correction had a very small effect on the predicted rate coefficients.)

Lennard-Jones parameters[27] (summarized in Table 1) were used to compute the CH_4 + M collision frequencies Z using the usual combining rules; the arithmetic mean of the collision radii and the geometric mean of the well depths were used. Classical trajectories were used to calculate $\alpha(T)$, as described in detail in Sec. II.B. ME calculations were carried out using Variflex.[28] Association rate coefficients (k_a) were obtained by converting the dissociation rate coefficients via the calculated equilibrium constant.

II.B. Classical trajectories

Direct dynamics. Full-dimensional direct dynamics trajectory calculations were used to study energy transfer for the He, Ne, H_2, and CH_4 baths. These simulations included thousands of trajectories for each bath gas, and thousands of gradient evaluations were required for each trajectory. The level of electron correlation and the size of the basis set that could be used to describe the molecular forces in the direct dynamics trajectory calculations were therefore limited to methods that could affordably be used for $\sim 10^7$ gradient calculations. The strategy adopted here was to use high-level ab initio calculations (counterpoise corrected QCISD(T) calculations with complete basis set (CBS) extrapolations based on the aug-cc-pVDZ and aug-cc-pVTZ basis sets) to evaluate the accuracy of lower-level quantum chemistry methods with efficiencies suitable for direct dynamics.

The accuracies of the lower-level direct dynamics potential energy surfaces were evaluated by considering interaction energies along three to nine CH_4–M approaches and calculating the following errors relative to the QCISD(T)/CBS energies: $\varepsilon_{\rm min}$, the root-mean-squared error in the minimum energy along each approach; $\varepsilon_{\rm rep}$, the root-mean-squared error in the center of mass separations at 2000 cm^{-1} up the repulsive wall along each approach; and $\varepsilon_{\rm rel} \equiv \varepsilon_{\rm min}/V_{\rm min}$, a relative error in the well depth, where $V_{\rm min}$ is the QCISD(T)/CBS van der Waals well depth for the most favorable approach. For the atomic baths, three approaches of M to CH_4 (fixed at its classical equilibrium geometry) were considered, with "face" and "vertex" denoting approaches along a C_3 axis with M equidistant from the nearest 3 and 1 H atoms on CH_4, respectively, and "edge" denoting a C_2 approach bisecting two H atoms on CH_4. For the diatomic baths, face, vertex, and edge approaches of the center of mass of M to CH_4 were considered for two or three orientations of the bath gas for a total of six or nine approaches. For M = CH_4, three approaches were considered: a face–face approach, a face–vertex approach, and a vertex–vertex approach. The errors in the direct dynamics and approximate potential energy surfaces discussed throughout Sec. II.B are summarized in Table 2; figures comparing QCISD(T)/CBS interaction energies with the lower-level direct dynamics and approximate potential energy surfaces for all the bath gases considered here are provided as supporting information.

A direct dynamics trajectory study of energy transfer in CH_4 for M = He was previously reported[10] using the MP2/aug'-cc-pVDZ potential energy surface, where it was shown to predict interaction energies in good agreement with QCISD(T)/CBS energies, as reproduced in Fig. 1(a). For He, the average error in the well depth $\varepsilon_{\mathrm{min}}$ for the MP2/aug'-cc-pVDZ method is only 4 cm^{-1}, and the error in the repulsive wall distance $\varepsilon_{\mathrm{rep}}$ is 0.04 Å. The accuracy of the MP2/aug'-cc-pVDZ method was further tested here for M = Ne, CH_4, and H_2. Agreement between the MP2/aug'-cc-pVDZ and QCISD(T)/CBS interaction energies is excellent for Ne ($\varepsilon_{\mathrm{min}}$ = 5 cm^{-1}; $\varepsilon_{\mathrm{rep}}$ = 0.02 Å) and CH_4 ($\varepsilon_{\mathrm{min}}$ = 10 cm^{-1}; $\varepsilon_{\mathrm{rep}}$ = 0.01 Å). For M = H_2, interaction energies were considered where the bath gas was oriented either radially (i.e., along the direction of the approach) or perpendicular to the direction of approach for a total of six CH_4–M approaches. The MP2/aug'-cc-pVDZ method performs less well for H_2 than for He, Ne, and CH_4, although the agreement is still good with $\varepsilon_{\mathrm{min}}$ = 24 cm^{-1} and $\varepsilon_{\mathrm{rep}}$ = 0.04 Å. A simple empirical improvement to the MP2/aug'-cc-pVDZ potential for M = H_2 was made by “scaling all correlation”[29] (SAC), where $E_{\mathrm{SAC}} = E_{\mathrm{HF}} + (E_{\mathrm{MP2}} - E_{\mathrm{HF}})/F$, E_{MP2} and E_{HF} are MP2/aug'-cc-pVDZ and HF/aug'-cc-pVDZ energies, and F = 0.8 is an empirical parameter. The SAC method more accurately describes the depth of the van der Waals well and the range of the repulsive wall, with $\varepsilon_{\mathrm{min}}$ = 11 cm^{-1} and $\varepsilon_{\mathrm{rep}}$ = 0.02 Å. These errors are reduced by a factor of two relative to those for the unscaled MP2 surface; the difference in the computational costs of the MP2 and SAC methods is negligible.

The use of the MP2 and SAC methods with double-zeta basis sets is a compromise between accuracy and computational efficiency. We emphasize that the MP2 interaction potentials are *not* converged with respect to the completeness of the basis set at the aug'-cc-pVDZ level and that using larger basis sets can reduce the accuracy of the MP2 method relative to QCISD(T)/CBS. (However, MP2/CBS agrees well with QCISD(T)/CBS for these systems.) On the other hand, MP2 has significant advantages over less rigorous methods such as Hartree-Fock and semiempirical methods, because it includes dynamical correlation, which is important for describing long-range forces. In fact, in tests not described in detail here, the MP2/aug'-cc-pVDZ method was found to perform significantly better than double-zeta basis set calculations using HF and several DFT methods, including DFT methods specifically designed for describing dispersion interactions. Semiempirical methods (AM1, PM3, etc.) are not suitable for describing dispersion interactions and were not considered for the full dimensional direct dynamics calculations. Note that the quantitative adjustment made using the SAC approach for H_2 results in a refinement of the well depth by only 30 cm^{-1}, which rivals the mean accuracies of the best empirically adjusted DFT methods designed to model dispersion.[30]

A separable approximation to the potential energy surface. While MP2 is an accurate and fairly efficient choice for the systems discussed above, and while we are most interested in computing highly averaged quantities using ensembles of only several hundreds of trajectories, direct dynamics can nonetheless be computationally prohibitive for many systems of interest. It is therefore desirable to test more efficient methods for describing the potential energy surface for use in larger systems. Direct dynamics calculations using the MP2 and SAC methods discussed above provide benchmark results for validation studies of the approximate potentials discussed next.

The full-dimensional CH_4 + M potential energy surface can be written

$$V(\mathbf{R}) = V_{\mathrm{T}}(\mathbf{R}_{\mathrm{T}}) + V_{\mathrm{M}}(\mathbf{R}_{\mathrm{M}}) + V_{\mathrm{T-M}}(\mathbf{R}), \qquad (21)$$

where V_{T} is the intramolecular potential energy surface of the target (CH_4) and is a function of the internal coordinates of CH_4 ($\mathbf{R}_{\mathrm{T}}$), V_{M} is the internal potential energy for the bath gas ($V_{\mathrm{M}} = 0$ for atomic baths) and is a function of the internal coordinates, if any, of the bath ($\mathbf{R}_{\mathrm{M}}$), and $V_{\mathrm{T-M}}$ is the intermolecular potential and is rigorously a function of all of the internal coordinates of CH_4 + M ($\mathbf{R}$). Here we test the accuracy of further approximating the interaction potential $V_{\mathrm{T-M}}$ as a sum of pairwise atom-atom interactions, i.e.,

$$V_{\mathrm{T-M}}(\mathbf{R}) \approx \sum_i V_2(R_i), \quad (22)$$

where i labels pairs of intermolecular atoms, and R_i is their separation. Equation 22 neglects higher order terms (e.g., $V_3(R_i,R_j,R_k)$, etc.) in the interaction potential that are responsible for screening, valence saturation effects, etc. Two forms for V_2 were considered: the Lennard-Jones (LJ) potential

$$V_2(R_i) = D_a\left[(R'_a/R_i)^{12} - 2(R'_a/R_i)^6\right] \quad (23)$$

and a modified Buckingham (exp/6) potential

$$V_2(R_i) = A_a \exp(-R_i/B_a) - C_a^6/(R_i^6 + S_a^6), \quad (24)$$

where the subscript a indicates that the fitted parameters depend on the identities of the atoms in the ith pair (i.e., a = C–He, H–He, etc). We refer to approximations in eqs 21 and 22 are referred to as the "separable pairwise" approximation to the interaction potential. This approximation (along with either the LJ or exp/6 functional forms for V_2) is almost always employed in trajectory studies of energy transfer. The only exception we are aware of is our own previous study of CH_4 + He.[10] The flexibility and fitting accuracy of the separable pairwise approximation is first discussed by comparing the fitted surfaces with the accurate QCISD(T)/CBS energies. The fitting errors are summarized in Table 2.

For He and Ne, exp/6 parameters for eq 24 were obtained by fitting $V_{\mathrm{T-M}}$ to QCISD(T)/CBS energies along three CH_4–M approaches. Alexander and Troya's[31] parameterizations (fit to fp-CCSD(T)/CBS energies) were used for Ar and Kr. The separable pairwise approximation with the exp/6 form for V_2 very accurately describes the QCISD(T)/CBS energies for He (Fig. 1(b)) and for the other the atomic baths, with well depth errors of only 1–8 cm^{-1} (4–7%) and repulsive wall distance errors of 0.03–0.04 Å.

The LJ separable pairwise approach (eq 23) was considered for He, with parameters obtained by fitting to the QCISD(T)/CBS results. This fit is labeled LJ-A and is shown in Fig. 1(c). A Lennard-Jones interaction potential based on tabulated[32] parameters (labeled LJ-B) was also considered; this parameterization is shown in Fig. 1(d). The LJ-A fit is fairly accurate in the region of the van der Waals well ($\varepsilon_{\mathrm{min}}$ = 1.8 cm^{-1}) but is unable to accurately describe the shape of the repulsive wall, leading to large errors in the repulsive wall distances at interaction energies of 2000 cm^{-1} ($\varepsilon_{\mathrm{rep}}$ = 0.3 Å).

The Lennard-Jones fit based on the tabulated parameters somewhat less poorly fits the range of the repulsive walls ($\varepsilon_{\text{rep}} = 0.1$ Å) but overpredicts the depths of the van der Waals wells ($\varepsilon_{\text{min}} = 7.0\ \text{cm}^{-1}$). The LJ form for V_2 is clearly less accurate than the exp/6 form, and eq 23 was not considered for the other baths.

Next, we consider the flexibility of the exp/6 separable pairwise approach for the diatomic baths. As discussed above, six cuts through the CH_4–M interaction potential were considered for H_2, three radial approaches and three perpendicular approaches. The exp/6 separable pairwise model was found to be unable to globally describe the orientation dependence of H_2 accurately, as shown in Fig. 2. Three parameterizations of the exp/6 model were therefore obtained: a compromise fit to both the perpendicular and radial data (PR), a fit to the radial data only (R), and a fit to the perpendicular data only (P). In the compromise fit (Fig. 2(a) and 2(b)), the well depth is accurately described only on average, and the fit fails to prefer radial orientations. The repulsive wall distances are somewhat shorter-ranged than the QCISD(T)/CBS energies for the radial approaches, as well. Good accuracy was obtained when fitting only one set of approaches (as in the R or P fits), but the resulting fits performed poorly for the set of approaches not included in the fitting data (cf. Figs. 2(c)–2(f)), with well depth errors of 50–75 cm^{-1}. As shown in Table 2, all three fits have similarly large errors averaged over all six approaches, with errors 2–6 larger than those for the SAC direct dynamics potential discussed above. Nonpairwise corrections to eq 22 to more accurately describe the orientation dependence were not pursued here.

Poor performance of the exp/6 separable pairwise approach was also obtained for the N_2 and CO baths. The N_2 and CO baths both feature prereactive complexes that appear as relatively deep wells in radial approaches to a vertex (i.e., directly to an H atom) of CH_4. (The associated abstraction reaction channels, e.g., $CH_4 + CO \rightarrow CH_3 + HCO$, are not open at the energies considered here.) These features further degraded the accuracy of the separable pairwise strategy for N_2 and CO, with well depth errors of as much as 100 cm^{-1} for some approaches. Again, three fits for N_2 were obtained: a compromise (RP) fit, a radial-data-only (R) fit, and a perpendicular-data-only (P) fit. The errors for the three fits are summarized in Table 2, where the average relative error in the well depths and the average error in the repulsive wall distances are shown to be somewhat smaller than for H_2. For CO, two sets of radial approaches were considered to evaluate the approximate potential energy surfaces, with either the C or the O atom on CO oriented toward CH_4, for a total of nine approaches. The exp/6 fits for CO were found to be especially poor, as shown in Table 2, with very large errors in the repulsive wall distances ($\varepsilon_{\mathrm{rep}}$ = 0.1–0.4 Å) and large relative errors in the well depths of 20–40%.

The fitted parameters for $V_{\mathrm{T-M}}$ for the atomic and diatomic baths are provided as supporting information. A separable pairwise fit for M = CH_4 was not pursued.

For H_2, V_{M} was fit to the calculated curve of Kołos and Wolniewicz.[33] For N_2, V_{M} was fit to full valence MRCI+Q/CBS calculations; the calculated curve agrees well with the curve reported by Le Roy et al.[34] For CO, V_{M} was fit to RKR data[35] and the experimental dissociation energy.[25]

We considered three methods for calculating V_{T}, the intramolecular potential of CH_4: MP2/aug'-cc-pVDZ and the semiempirical extended Hückel[36] or tight binding[37] (TB) model for hydrocarbons of Wang and Mak.[38,39] The TB model features a minimal orbital description of only 4 orbitals for C and 1 for H, parameterized matrix elements for the molecular Hamiltonian, parameterized core-core repulsion, and a single (i.e., noniterative) 8x8 matrix diagonalization for each gradient evaluation. The TB calculations are several orders of magnitude faster than the MP2/aug'-cc-pVDZ calculations. The vibrational frequencies and rotational constants for CH_4 predicted by the TB, MP2, and SAC methods are compared with experimental values in Table 3. Agreement with the experimental values is generally good, although the TB method overpredicts the vibrational frequencies.

When trajectory results calculated using the separable pairwise strategy are presented, the results will be labeled "A+B," where A is the method used to calculate V_{T} and B is the method used to calculate $V_{\mathrm{T-M}}$, e.g., MP2+exp/6 indicates that MP2 was used to describe the CH_4 potential and eq 24 was used to describe the bath gas interaction. The label "MP2" by itself indicates a nonseparable, full-dimensional direct dynamics calculation using the MP2/aug'-cc-pVDZ method (or, for M = H_2, the SAC variant discussed above).

Initial conditions for single temperature ensembles. Energy transfer was studied using ensembles of 500–5000 trajectories prepared at fixed bath gas temperatures T from

300–4000 K. A scheme for preparing ensembles of CH_4 + He collisions appropriate for calculating energy transfer parameters relevant to the ME energy transfer models discussed above has been described previously.[10] Briefly, trajectories were prepared with a thermal distribution of the initial collision energy E'_c and for fixed initial rotational states J'. The initial vibrational energy E'_{vib} was chosen to be a function of J' and close to the rotationally adiabatic dissociation threshold $E_{J'}$, with the initial geometries and momenta determined microcanonically. Four modifications were made for the present study.

First, the strategy was generalized to handle molecular baths. The initial internal coordinates and vibrational and rotational momenta of the molecular bath were selected randomly and evenly in time from separate equilibration runs carried out for the isolated molecular bath gas using an Andersen thermostat[40] set to T. For the diatomic baths, a more rigorous approach of selecting the initial vibrational and rotational states from independent, thermal, quantum mechanical distributions was also tested. These two sampling schemes (which may be called "classical" and "quasiclassical," respectively) gave energy transfer results within the reported statistical uncertainties, and results obtained using classical sampling are presented here.

Second, the impact parameter b was sampled evenly from 0–b_{max}, whereas in the previous study b^2 was sampled evenly from $0\text{–}b^2_{\text{max}}$. The new scheme intentionally artificially oversampled small b, and this bias was corrected when calculating energy distribution moments, as discussed below and elsewhere.[41] This scheme was motivated by the observation that large impact parameter trajectories, which are sampled most often in the unbiased sampling procedure, tend to contribute less to the overall energy transfer averages than small impact parameter collisions.

Third, the initial rotational state of CH_4, J', was sampled from a thermal distribution at T. In the previous work, ensembles of trajectories were prepared with fixed values of J', and the resulting J'-dependent energy transfer averages were subsequently averaged over J'.

Fourth, the initial vibrational energy E'_{vib} of CH_4 was set to

$$E'_{\text{vib}}(J') = 0.95\,E_{J'} \qquad (25)$$

where $E_{J'}$ is the threshold vibrational energy for rotationally adiabatic dissociation for CH_4, and the rotational thresholds were determined for $K = 0$. Previously, the initial vibrational energy was set to 95% of the average of the rotational thresholds for $K = 0$ and $K = J$. This change corresponds to a very small difference in the initial energy and has a negligible effect on the predicted energy transfer averages.

Final state analyses. The final CH_4 + M separation was chosen to be suitably large (6–8 Å) so that the final internal energy, E, and final total angular momentum, J, of CH_4 could be calculated unambiguously. With the change in the internal energy of CH_4 given by $\Delta E = E - E'$, the ensemble-averaged energy transfer moments were calculated as follows

$$<\Delta E> = \frac{Z_{\mathrm{HS}}}{Z_{\mathrm{LJ}}} \sum_{i=1}^{N} w_i^b \Delta E_i / N, \tag{26}$$

$$<\Delta E^2>^{\frac{1}{2}} = \sqrt{\frac{Z_{\mathrm{HS}}}{Z_{\mathrm{LJ}}} \sum_{i=1}^{N} w_i^b \Delta E_i^2 / N}, \tag{27}$$

$$<\Delta E_{\mathrm{d}}> = -\frac{Z_{\mathrm{HS}}}{Z_{\mathrm{LJ}}} \sum_{i=1}^{N} w_i^b \min(\Delta E_i, 0) / N_{\mathrm{d}}, \tag{28}$$

where Z_{HS} and Z_{LJ} are the hard sphere and Lennard-Jones collision frequencies (calculated using the parameters in Table 1 and the usual combining rules), respectively, N is the size of the ensemble, and N_{d} is the number of deactivating collisions. The weights

$$w_i^b = \frac{b_i}{<b>} = \frac{2b_i}{b_{\max}} \tag{29}$$

correct for the artificial sampling of the impact parameter b, as discussed above. One-sigma uncertainties are reported for the average energy transfer parameters, as estimated using the bootstrap resampling method.[42,43]

The per-collision averages in eqs 26–29 are scaled to the Lennard-Jones collision rates Z_{LJ}. We also consider first order average energy transfer rates (i.e., per-time averages), defined

$$<r> \equiv Z_{\mathrm{LJ}} <\Delta E> n_{\mathrm{M}} \tag{30}$$

$$<r_{\mathrm{d}}> \equiv Z_{\mathrm{LJ}} <\Delta E_{\mathrm{d}}> n_{\mathrm{M}} \tag{31}$$

$$<r^2>^{1/2} \equiv Z_{\mathrm{LJ}} <\Delta E^2>^{1/2} n_{\mathrm{M}}. \tag{32}$$

These quantities have the units of energy transferred per unit time, which we will express as cm^{-1}/s. The average energy transfer rates in eqs 30–32 are independent of the choice for the Lennard-Jones collision frequency. Note that the bath gas concentration n_{M} is related to the temperature T and pressure p via the ideal gas law, $n_{\mathrm{M}} = p/k_{\mathrm{B}}T$, and Z_{LJ} is a function of T; the averages of ΔE (eqs 26–28) therefore dependent differently on temperature than the average rates r (eqs 30–32). The present trajectory approach is closely related to that of Lim and Gilbert,^{44} who also recognized that, by considering highly averaged quantities, small ensembles of trajectories could be useful in parametrizing energy transfer models in master equation calculations. Furthermore, they pointed out the usefulness of considering energy transfer rates (30–32) instead of the more commonly considered per-collision energy transfer averages (26–28).

Multitemperature ensembles. The single temperature ensembles described above consist of trajectories with thermal distributions of J' and E'_c for some bath gas temperature T. The same ensemble of trajectories could be used to calculate energy transfer averages at a different temperature T_2 by assigning weights to each trajectory based on the relative thermal populations of J' and E'_{c} at T and T_2. This idea was generalized here to calculate energy transfer averages over a range of bath gas temperatures using a single ensemble of trajectories as follows.

For each trajectory in a multitemperature ensemble, a sampling temperature, T_{s}, was selected randomly and evenly from $T_{\min}$ to $T_{\max}$. The initial rotational state and relative collision energy were then chosen from appropriate thermal distributions for the sampling temperature T_{s}. The resulting ensembles were used to calculate energy transfer averages any temperature T by weighting each trajectory by

$$w_i^T = \frac{P_J(T;J_i')P_{\mathrm{c}}(T;E_{\mathrm{c},i}')}{\int\limits_{T_s=T_{\min}}^{T_{\max}} dT_s P_J(T_s;J_i')P_{\mathrm{c}}(T_s;E_{\mathrm{c},i}')/(T_{\max}-T_{\min})}, \tag{31}$$

in eqs 26–28, where P_J and P_{c} describe thermal distributions of the initial rotational state and relative collision energy, respectively. This scheme does not introduce any additional approximations and may be more useful than sampling at fixed values of T.

Somewhat more complicated distributions of T_{s} could be used to produce ensembles with energy transfer moments with equal relative statistical uncertainties over the entire temperature range T_{min} to T_{max}. In the current strategy, the relative statistical uncertainties are roughly twice as large at the edges of the temperature range than at intermediate temperatures.

Trajectory calculations were carried out using the freely available direct dynamics trajectory code DiNT[45] interfaced with the Molpro program package.[46] Ensemble sizes were chosen such that the direct dynamics ensembles had relative errors of ~10% (100–2000 trajectories) and the less expensive TB+exp/6 ensembles had relative errors of a few percent (5000–20000 trajectories).

III. Results and Discussion

III.A. Tests of the separable potential approximation

Energy transfer averages were previously reported[10] for He using a full dimensional MP2/aug'-cc-pVDZ potential energy surface. These calculations were repeated for the present study to confirm the accuracy of the new sampling procedures; the present MP2 results for $<\Delta E_{\mathrm{d}}>$ at 300–2000 K are ~20% higher than the previously published results due to the improved sampling over J' employed here. These differences are small and close to the combined statistical uncertainties in the MP2 calculations in the present and previous studies.

A comparison of the predicted values for $<\Delta E_{\mathrm{d}}>$ for M = He calculated using the full dimensional MP2 method as well as several separable pairwise potential energy surfaces is shown in Fig. 3. The Lennard-Jones approximation for the intermolecular potential performs very poorly relative to the MP2 results. The LJ-A potential, which was parameterized to fit the van der Waals well, overestimates $<\Delta E_{\mathrm{d}}>$ by 120–150%. Using tabulated values for the Lennard-Jones parameters, the LJ-B potential overestimates $<\Delta E_{\mathrm{d}}>$ by 70% at 300 K and by almost a factor of 3 at 1150 and 2000 K. As discussed in Sec. II.B., neither Lennard-Jones potential accurately describes the repulsive wall (the LJ interaction is “harder” than the accurate interaction), and this deficiency introduces considerable error into the calculated results. It is likely that these deficiencies in the LJ potential for modeling the repulsive wall are general, and one can conclude that LJ interactions cannot be used for accurate energy transfer studies.

The exp/6 separable pairwise model was tested against the full-dimensional MP2 direct dynamics calculations for two atomic baths (He and Ne), and comparisons of $<\Delta E_d>$ calculated using the MP2 and MP2+exp/6 potential energy surfaces are shown in Figs. 3 and 4 for He and Ne, respectively. The predicted values of $<\Delta E_d>$ obtained using the MP2+exp/6 potential energy surfaces are in excellent agreement with the full dimensional direct dynamics results, differing from one another at 1150 and 2000 K by less than 15%. The relative differences between the MP2 and MP2+exp/6 predictions are larger at 300 K, although the differences (~30%) are close to the estimated 1σ statistical uncertainties. These results suggest that the neglect of many-body terms in eq 22 is not a significant source of error for the atomic baths, so long as accurate repulsive walls, such as those in the fitted exp/6 potential energy surfaces, are used. The good performance of the exp/6 parameterizations is consistent with the small fitting errors of the exp/6 interaction potential, which accurately describes both the depth of the van der Waals well and the shape of the repulsive wall.

For both He and Ne, the predicted energy transfer averages were found to be insensitive to the level of theory used to describe the target potential energy surface V_T, with the MP2+exp/6 and TB+exp/6 values for $<\Delta E_d>$ differing by only 5–15%. This result is perhaps surprising; the TB method overpredicts the vibrational frequencies for CH_4, as shown in Table 3, such that the rotationless harmonic density of states at the dissociation threshold for the TB potential is 40% smaller than that for the MP2 surface. This result is encouraging, as the Wang and Mak TB parameterization predicts fairly accurate structures and frequencies for a variety of hydrocarbons[38] and is very efficient in the trajectory calculations.

The results obtained using the multitemperature sampling scheme are in excellent agreement with the single temperature strategy, as shown in Figs. 3 and 4, and the multitemperature scheme provided more precise results for a fixed total number of trajectories. For example, with ensemble sizes of 120, 340, 575, and 1100 CH_4 + He trajectories for 300, 1150, 2000, and 4000 K, respectively, the MP2 results has relative 1σ errors of ~15%. In contrast, a 2000 trajectory ensemble using the multitemperature strategy predicted results with 1σ errors of only 5–10% over the temperature range 300–

4000 K. The improved statistics facilitated the present comparisons of the various potential energy surfaces for the atomic baths.

Next, we compare the TB+exp/6 separable pairwise method with full dimensional SAC calculations for the diatomic bath, H_2. As discussed above and in contrast to the atomic colliders, the pairwise exp/6 functional form is not flexible enough to describe the orientation dependence interaction potential, and three exp/6 parameterizations (R, P, and RP) were obtained. The values of $<\Delta E_\mathrm{d}>$ predicted by the three exp/6 fits are compared with the full dimensional SAC results in Fig. 5. The compromise fit (exp/6 RP) predicts values of $<\Delta E_\mathrm{d}>$ that are ~25% lower than the SAC results, whereas the exp/6 R predictions are in good agreement with the SAC results. The exp/6 P fit is accurate at elevated temperatures but performs less well at 300 K. It is difficult to rationalize these results based on the quality of the three exp/6 parameterizations summarized in Table 2; the RP parameterization more accurately fits the range of the repulsive walls than the R and P parameterizations, and all three have similarly poor descriptions of the well depths, on average. We conclude that it is likely that the good agreement of the exp/6 R fit with the SAC results is accidental, and that the range of results obtained from the exp/6 fits is representative of an additional uncertainty in the predicted exp/6 results due to the separable pairwise approximation for H_2.

Although we do not have full dimensional MP2 trajectory results for M = N_2 and CO, we can gain further insight into the accuracy of the separable pairwise approximation for the diatomic baths by comparing the results of several reasonable exp/6 parameterizations for N_2 and CO. As discussed above, three exp/6 fits for N_2 were obtained. For CO, we consider only the best two exp/6 fits: the compromise (RP) fit and the fit to the radial (R) data with the O atom facing CH_4. Predicted values of $<\Delta E_\mathrm{d}>$ for the exp/6 fits for N_2 and CO are shown in Fig. 6. The N_2 results differ from one another by only ~10%, whereas the CO results differ from each other by 25–50%. Again, the relative magnitudes of these uncertainties in $<\Delta E_\mathrm{d}>$ do not appear evident from the quality of the fitted potentials for N_2 and CO indicated by the errors shown in Table 2.

The sensitivity of calculated energy-transfer averages to properties of the potential energy surface used in trajectory calculations has been studied previously. In these previous studies, the predicted energy transfer averages were found to be largely insensitive to the potential energy surface used to describe the target and to depend sensitively on the functional form used to describe the interaction potential and, in particular, on the range and "softness" of the repulsive wall.[12,14,44,47,48,49] The present results agree with these qualitative conclusions. The full dimensional MP2 and SAC direct dynamics calculations reported here allow us to further quantify the errors associated with the use of approximate potential energy surfaces, at least for CH_4 + M. For the atomic baths, the neglect of nonpairwise terms in the interaction potential introduces a negligible uncertainty into the predicted energy transfer averages so long as parametrized exp/6 pairwise interactions are used. The use of LJ pairwise interactions leads to significant errors and is not appropriate for quantitative or even semiquantitatve studies. For the diatomic baths, on the other hand, the exp/6 separable pairwise strategy is not flexible enough to describe the interaction potential accurately. The resulting ambiguities in the fitted parameters introduce an additional uncertainty of up to 50% into the predicted energy transfer averages for the diatomic baths. Unfortunately, the quality of the calculated energy transfer averages is not evident from the quality of the fitted interaction potentials, at least not from the simple errors summarized in Table 2. Finally, we note that additional uncertainties may be expected when applying the separable pairwise strategy to targets that are less spherical than CH_4, even for atomic baths, as these systems may have a more complicated interaction potential orientation dependence.

III.B. A comparison of the baths

Next, a comparison of the relative energy transfer efficiencies of the eight baths is made. The average energy transferred in deactivating collisions $<\Delta E_d>$ calculated using the TB+exp/6 method is shown at 300 and 2000 K in Fig. 7 for the eight baths. Full dimensional direct dynamics results are also shown, if available. The MP2 and TB+exp/6 potential energy surfaces predict very similar values for $<\Delta E_d>$, with magnitudes that agree within the 1σ statistical uncertainties for He and Ne. As discussed above, the TB+exp/6 predictions for the diatomic baths have additional uncertainties of 10–50% due to ambiguities in the fitted surfaces. The diatomic baths have energy transfer averages similar in magnitude to those for the atomic baths, but the additional uncertainties for N_2

and CO preclude a quantitative comparison of their energy transfer efficiencies with the other baths.

At room temperature (Fig. 7(a)), the magnitude of $<\Delta E_\mathrm{d}>$ is very similar for all the baths except for CH_4, which transfers nearly three times as much energy, on average, in deactivating collisions. The predicted values for $<\Delta E_\mathrm{d}>$ are somewhat larger (by only 10–20 cm^{-1}) for H_2, Ar, and Kr than for He and Ne, with differences close to the statistical uncertainties.

The trend in $<\Delta E_\mathrm{d}>$ with respect to the bath gas differs at elevated temperatures. At 2000 K (Fig. 7(b)), He and H_2 are significantly stronger colliders than the other atomic and diatomic baths, transferring ~40% more energy on average per deactivating collision. He and H_2 transfer similar amounts of energy as one another, and, again, CH_4 is the strongest collider. The trajectory results indicate that the change in the relative energy transfer efficiencies occurs around 500 K, suggesting that room temperature relative efficiencies may not be useful predictors of relative efficiencies at combustion temperatures.

The results in Fig. 7 are scaled to Lennard-Jones collision frequencies, i.e., $<\Delta E_\mathrm{d}>$ is the average energy transferred per deactivating collision, assuming collisions are occurring at the Lennard-Jones collision rate. This choice, although conventional, is arbitrary. Furthermore, the accuracy of any particular set of the Lennard-Jones parameters and of the usual Lennard-Jones combining rules is unknown in the present context. Fig. 8 presents the same data as Fig. 7 but without scaling to Lennard-Jones collision frequencies, i.e., $<r_\mathrm{d}>$ is defined by eq 30 as the average 1st order energy transfer rate coefficient for deactivating collisions. At room temperature, Fig. 8 shows H_2 to be an especially efficient collider, with $<r_\mathrm{d}>$ more than twice as large for H_2 than for the atomic baths. Ne is a relatively poor collider, with the other atomic baths differing from one another by less than 10% in $<r_\mathrm{d}>$. At 2000 K, He is twice as efficient as Ne, Ar, and Kr, with H_2 again more efficient than the atomic baths. The predicted value for $<r_\mathrm{d}>$ for CH_4 is 70% larger than H_2 at 300 K, but the two baths predict similar values of $<r_\mathrm{d}>$ at 2000 K.

Overall, the trends in $<\Delta E_\mathrm{d}>$ and $<r_\mathrm{d}>$ are similar, but $<r_\mathrm{d}>$ may be expected to more clearly predict the quantitative kinetic effect of the different baths in promoting dissociation. The usefulness of considering the average energy transfer rate coefficients (in contrast to the per-collision energy transfer averages) has been emphasized by Lim and Gilbert.[19,44]

The relative collisional energy transfer efficiencies of typical bath gases are of considerable interest, though few systematic experimental or theoretical studies exist. As noted in the Introduction and discussed in detail by Gilbert,[19] in one set of trajectory studies for rare gas collisions with azulene at 300 K He was predicted to be the most efficient atomic collider in contrast to experimental results for the same system.[22] Good agreement between the experimental and theoretical results was obtained for the heavier atomic baths. Gilbert suggested that more accurate potential energy surfaces were needed for He. The present results for rare gas collisions with CH_4, using the interaction potential energy surfaces validated in Sec. III.A, predict He to be slightly less efficient than the other atomic baths at room temperature, which may support Gilbert's analysis. In another set of systematic experimental studies, Michael and co-workers measured a series of low pressure rate coefficients for NO_2, HO_2, HNO, HCO, and C_2H_5 recombination reactions in several baths.[23,50,51,52] In general, these studies found He, Ar, and Kr to have efficiencies similar to one another, Ne to be less efficient than the other atomic baths, and H_2 to be more efficient. The relative energy transfer efficiency of He was also shown by Michael et al.[52] to increase with temperature for NO_2 recombination at 200–500 K. These experimental trends are consistent with the present work. For N_2, however, the experimental work of Michael et al. generally found rate coefficients roughly twice as large as those for He, whereas in the present work the heavier diatomic baths are of similar efficiency as the heavier atomic baths. This discrepancy could indicate further uncertainties in the present trajectory calculations for diatomic baths due to the separable pairwise approximation for the interaction potential, as discussed above. Finally, we note again the temperature dependence in the relative collisional energy transfer averages shown in Fig. 7 may complicate attempts at generalizations about relative bath gas efficiencies.

Figure 9 summarizes $<\Delta E_d>$ and $<\Delta E^2>^{1/2}$ for M = He, Ne, Ar, and Kr (TB+exp/6), H_2 (SAC), CH_4 (MP2), and N_2 and CO (averaged over the several TB+exp/6 parameterizations). The relative bath gas efficiencies were discussed above, and here we focus on the temperature dependence of the predicted energy transfer averages. The data for $<\Delta E_d>$ were fit to the empirical formula in eq 1; both α_{300} and n were treated as adjustable parameters and were determined by minimizing the mean unsigned error to the data in Fig. 9. For the atomic baths, α_{300} = 104–123 cm^{-1} and n = 0.67–0.95, as shown in Table 4. These values are consistent with typical empirical determinations of α_{300} and n, where α_{300} = 50–300 cm^{-1} and $n \approx 1$.

The present data suggest a more complicated temperature dependence than is assumed in eq 1. The best fit parameters to eq 1 for the temperature range 300–2000 K underpredicted the calculated room temperature values of $<\Delta E_d>$ by 10–20% for the atomic baths. For the polyatomic baths, eq 1 was again unable to accurately describe the entire temperature range considered, and the optimized parameters summarized in Table 4 overpredicted the 1150 K data by as much as 15%. This more complicated temperature dependence than what is often assumed (as in eq 1) may contribute to the general difficulty in developing an intuition about how the parameters α_{300} and n depend on the bath gas and target.

The predicted values for $<\Delta E^2>^{1/2}$ (Fig. 9(b)) show a stronger temperature dependence than $<\Delta E_d>$. The relative ordering of the predicted values of $<\Delta E^2>^{1/2}$ for the eight baths at 300 and 2000 K is similar to that for $<\Delta E_d>$. Specifically, at 300 K, the values for $<\Delta E^2>^{1/2}$ for the atomic baths, N_2, and CO are similar (148–155 cm^{-1}), with $<\Delta E^2>^{1/2}$ only slightly larger for H_2 (162 cm^{-1}) and much larger for CH_4 (416 cm^{-1}). At 2000 K, the predicted values for the root-mean-squared energy transfer for He and H_2 (940 and 839 cm^{-1}) are larger than those for the other atomic ($<\Delta E^2>^{1/2}$ = 716, 604, and 572 cm^{-1} for Ne, Ar, and Kr) and diatomic baths ($<\Delta E^2>^{1/2}$ = 702 and 712 cm^{-1} for N_2 and CO). Again, CH_4 is the strongest collider with $<\Delta E^2>^{1/2}$ = 1146 cm^{-1} at 2000 K.

The average energy transferred in all collisions $<\Delta E>$ is negative or very close to zero for 300–2000 K, with similar magnitudes for all the baths except He, H_2 and CH_4; for these baths $<\Delta E>$ is somewhat more negative. The magnitude of $<\Delta E>$ is small (only tens of cm^{-1}) and is typically close to or smaller than the statistical uncertainties for the ensembles considered here. Significantly more trajectories would be required to calculate $<\Delta E>$ accurately enough to be used in collision models. We note that the average initial vibrational energy $<E'_{\mathrm{vib}}> \approx 4.5$ eV corresponds to an initial vibrational temperature of ~6000 K ($T_{\mathrm{vib}} = <E'_{\mathrm{vib}}>/k_{\mathrm{B}}N_{\mathrm{vib}}$, with $N_{\mathrm{vib}} = 9$). The initial rotational distribution for our ensembles is already in thermal equilibrium with the bath. The net energy transferred is therefore negative as the bath and the rotational degrees of freedom equilibrate the vibrational degrees of freedom, i.e., as the vibrational degrees of freedom cool. The small values of ΔE reflect the "weak" nature of these collisions, i.e., many collisions would be required to bring the vibrational energy into equilibrium with the bath.

Figure 10 presents $<r_{\mathrm{d}}>$ and $<r^2>^{1/2}$ for the same trajectory ensembles shown in Fig. 9. The trends in the energy transfer rates with respect to the bath gases shown in Fig. 10 are somewhat different than the trends in the per-collision averages shown in Fig. 9. First, $<r_{\mathrm{d}}>$ and $<r^2>^{1/2}$ are both inversely proportional to the reduced mass of the system (roughly proportional to $\mu^{-1/2}$ if μ is the CH_4–M reduced mass) for the series of atomic baths and for the series of diatomic baths. This dependence arises primarily due to the dependence of the collision frequency on the relative mass, which is not included in Fig. 9. Second, for systems with especially shallow van der Waals wells (He and H_2), the temperature dependence is positive, whereas the baths with relatively deep van der Waals wells show an increased relative importance at room temperature, leading to weak or negative temperature dependences. Third, the diatomic baths N_2 and CO are somewhat more efficient than the heavy atomic baths, despite having similar reduced masses and well depths. The energy transfer rate for CH_4 is even larger than the energy transfer for the diatomic baths, again despite having a similar well depth and a smaller reduced mass. This likely reflects the enhancement of energy transfer as the number of vibrational and rotational modes in the bath gas increases. Figs. 9 and 10 present the same data, but the simple trends identified here (those respect to the relative mass, the well depth, and the dimensionality of the bath gas) are more apparent in the energy transfer rates shown in Fig. 10.

III.C. Decomposition rate coefficients and a comparison with experimental rate coefficients for M = He, Ar, Kr, and CH_4

Decomposition rate coefficients were calculated using eq 1, the parameters summarized in Table 4 obtained from the trajectory ensembles described in Sec. III.B, and the ME approach discussed in Sec. II. Low pressure limiting rate coefficients k_0 near 2000 K and pressure dependent rate coefficients k at 300 and 1150 K are shown for eight baths in Fig. 11. The values for k_0 at 2000 K (Fig. 11(a)) differ by as much as a factor of 5, ranging from 0.3–1.6 x 10^{-4} cm^3 $molecule^{-1}$ s^{-1}. The differences in the decomposition rate coefficients due to the bath gases, of course, decrease as the rate coefficients approach the high pressure limit, as shown in the falloff rate coefficients in Figs. 11(b) and 11(c). As suggested by Figs. 7 and 8, the relative efficiencies of the bath gases change as a function of temperature; this is evident in the different ordering of the association and dissociation rate coefficients with respect to the bath gas at 300 and 1150 K in Figs. 11(b) and 11(c), respectively. The trends in the effect of the eight baths on k are well reproduced by the trends in the average energy transfer rate coefficients shown in Fig. 10; these trends are more closely related to the trends in the average energy transfer rates than the per-collision energy transfer averages shown in Fig. 9 as suggested by eq 20 and elsewhere.[19,44] We emphasize that the energy transfer rate coefficients can be obtained just as easily from the trajectory calculations as the energy transfer averages.

Next, the present decomposition rate coefficients for M = He, Ar, Kr, and CH_4 are compared with available experimental results. In Fig. 12(a), the predicted results for k_0 in Ar are compared with experimental values from several groups[53,54,5556,57] and with the recommended value of Baulch et al.[58] The present prediction for Ar is ~25% lower than the recommended value, which was based largely on the measured rate coefficients of Kiefer and Kumaran[55] and agrees well with Hartig et al.[53] and Koike et al.[56] The most recent measurement (Sutherland et al.[57] in Kr) and the revised measurement from Davidson et al.[54] are somewhat lower and are in better agreement with the predicted results. Overall, the agreement between the predicted and measured values for k_0 in Ar is excellent.

In Fig. 12(b), the present predicted values of k in Ar near 1100 K are compared with the experimental falloff results of Barnes et al.[59] and with the recommended values of Baulch et al.[58] The predicted values of k are again lower than the measured and recommended rate coefficients, with the differences as large as a factor of two. The present theoretical predictions underestimate both the low pressure and falloff experimental rate coefficients. As discussed by Troe,[1] the low-pressure limit rate coefficient is approximately proportional to the density of states at threshold, and anharmonic vibrational corrections to the RRHO density of states would tend to increase the density and therefore the rate coefficient. Nguyen and Barker[60] calculated an anharmonic correction to the density of states for several systems including CH_4. At threshold for dissociation, this correction is close to a factor of two, in agreement with empirical corrections calculated and tabulated by Schmatz.[61] We approximated such an anharmonic correction to the density of states for CH_4 by scaling all of the harmonic frequencies by 0.91. This scaling doubled the rotationless harmonic density of states at the dissociation threshold. The equilibrium constant and partition functions were not scaled, such that the high pressure limiting rate coefficients were not affected. As seen in Fig. 12(a), the low pressure rate coefficient is doubled when the threshold density of states is doubled, consistent with Troe's analysis. The resulting values of k_0 obtained, however, overestimate the recommended values of k_0 by ~50% and are in worse agreement with experiment than the harmonic calculation. On the other hand, including the effect of anharmonicity significantly improves the agreement of the predicted results with the experimental falloff rate coefficients in Fig. 12(b), although the predicted rates are still somewhat too low.

In Fig. 13, falloff rate coefficients for CH_4 (+ CH_4) $\rightleftarrows$ CH_3 + H (+ CH_4) are compared with the measured rate coefficients of Barnes et al.[59] and Chen at al.[62] and with the recommended values of Baulch et al.[58] The predicted values are in good agreement with the measured rate coefficients and, on average, somewhat underpredict the measured values. Approximately correcting for the vibrational anharmonicity of CH_4 increases the predicted decomposition rate coefficients by up to a factor of two, but in this case it is unclear whether or not this adjustment systematically improves the agreement with the experimental results. In fact, the adjustment is close to the recommended uncertainty of Baulch et al.[58] ($\Delta\ln k_0 = \pm 0.3$).

We previously showed[10] that using direct dynamics trajectory ensembles to predict α for M = He and RRHO estimates for the CH_4 density of states resulted in association and decomposition rate coefficients for CH_4 that were in close agreement with experimental results.[59,63] A similar comparison is made in Fig. 14, where the newly predicted values for α for He are used. As indicated above, the present values for α are in good agreement with those from the previous study, and the resulting rate coefficients are again in good agreement with the experimental rate coefficients and with the recommended values of Baulch et al.[58] Scaling the frequencies to double the density of states at threshold worsens the agreement with the measured rate coefficients, although the high temperature (1150 K) results are perhaps equally well reproduced with and without scaling the harmonic frequencies.

We note that the present procedure of scaling the harmonic frequencies to approximate the effect of anharmonicity at the dissociation threshold does a poor job describing the density of states at intermediate and low energies and therefore introduces some additional error into the falloff calculations in Figs. 12–14. This error is mitigated somewhat as the high pressure limiting rate coefficients are not affected by this scaling. Despite these qualifications, these results suggest that errors in calculating the density of states using the RRHO approximation can be more significant than errors in the energy transfer models or in α at intermediate and low pressures. Furthermore, it is not clear from the present comparisons with experimental rate coefficients for He, Ar, and CH_4 whether or not such an adjustment systematically improves the predicted rate coefficients.

Overall, agreement between the predicted and measured rate coefficients is good (equally so, with or without correcting for anharmonicity), demonstrating the predictive usefulness of the present energy transfer models and of trajectory-based calculations of energy transfer parameters. Likewise, the present results confirm the accuracy of the recommended experimental values,[58] with the possible exception of the falloff rate coefficients for M = Ar, where the recommended and experimental values are somewhat higher than the theoretical rate coefficients. We note that Golden[15] recently discussed difficulties consistently modeling the experimental results for Ar using the ME and empirical values for α.

IV. Conclusions

Energy transfer in highly vibrationally excited CH_4 for eight baths was studied using classical trajectories. Direct dynamics calculations were carried out using validated, full-dimensional MP2 potential energy surfaces for M = He, Ne, H_2, and CH_4. These results were used to test the accuracy of representing the interaction potential as a separable sum of pairwise interactions. For atomic baths, this approximation was found to be very accurate so long as an exponential form was used to describe the repulsive wall. The use of a Lennard-Jones interaction potential led to significant errors in the theoretical predictions, overpredicting energy transfer averages by up to a factor of three. For diatomic baths, the separable pairwise approximation was not flexible enough to describe the dependence of the interaction potential on the orientation of the bath gas. The resulting ambiguity in the fitted parameters contributed an additional uncertainty of 10–50% to the predicted energy transfer averages. The separable pairwise approximation has been used in almost every study of energy transfer in the literature, and the present results suggest that such an approach may not be suitable for quantitative predictions for some systems.

A sampling scheme for using a single ensemble of trajectories to calculate energy transfer properties for a range of bath gas temperatures was introduced for atomic baths. The multitemperature sampling was shown to give more precise averages over a broader range of temperatures than the single temperature ensembles, for a fixed total number of trajectories. More generally, the use of small ensembles of only several hundreds of direct dynamics trajectories (as suggested by Lim and Gilbert[44]) has been shown to provide results accurate enough for parametrizing energy transfer models for use in ME calculations.

In addition to considering per collision energy transfer averages, we discussed first order energy transfer rate coefficients. These rate coefficients are straightforward to calculate using ensembles of trajectories yet avoid the customary but often arbitrary scaling to Lennard-Jones collision rates. It was confirmed that the energy transfer rate coefficients more directly predicted the kinetic effect of the bath gases. Furthermore, the energy transfer rate coefficients may be more useful in rationalizing trends in the relative energy transfer efficiencies due to properties of the baths.

The temperature dependence of the average energy transferred in deactivating collisions $\alpha \equiv \langle \Delta E_\mathrm{d} \rangle$ for eight baths was discussed. This quantity is often used to parameterize models of energy transfer assuming the functional form in eq 1. The present results suggest a more complicated temperature dependence, particularly at low temperature. Furthermore, it was shown that the relative bath gas efficiencies change as a function of temperature. Together, these results suggest that relative room temperature values for α may not be directly useful in parametrizing energy transfer models intended for higher temperature applications, such as combustion processes.

Fully predictive (i.e., parameter-free) decomposition and association rate coefficients for CH_4 were calculated for all eight baths, and comparisons with available experimental results for M = He, Ar, Kr, and CH_4 were made. In general, the agreement between the predicted and experimental rate coefficients is excellent and is within the recommended factor of two experimental uncertainties. The good agreement validates both the simplified energy transfer models used in the ME calculations for these systems and the trajectory based determinations of the energy transfer parameters.

Finally, we noted that the present low pressure calculations may suffer uncertainties of close to a factor of two due to our present neglect of anharmonicity when calculating the density of states for CH_4. These uncertainties may be larger than the uncertainties associated with the energy transfer models and direct-trajectory-based parameterizations. Further progress toward predictive unimolecular kinetics will likely require anharmonic treatments for the density of states, such as the spectroscopic series approaches recently advocated by Barker[60] or the more approximate schemes of Troe and Ushankov[64] and Schmatz.[61]

Supporting Information

Fitted intermolecular potential energy surface parameters and figures comparing QCISD(T)/CBS interaction energies with several low-level direct dynamics and approximate potential energy surfaces.

Acknowledgments

This work is supported by the Division of Chemical Sciences, Geosciences, and Biosciences, Office of Basic Energy Sciences, U.S. Department of Energy. Sandia is a multiprogram laboratory operated by Sandia Corporation, a Lockheed Martin Company, for the United States Department of Energy under Contract No. DE-AC04-94-AL85000. J.A.M. was supported as part of the Combustion EFRC, an Energy Frontier Research

Center funded by the U.S. Department of Energy, Office of Science, Office of Basic Energy Sciences under Award Number DE-SC001198.

Table 1. Lennard-Jones collision frequency parameters

	σ, Å	ε, cm^{-1}
CH_4	3.746	98.28
He	2.576	7.089
Ne	2.749	24.74
Ar	3.330	94.87
Kr	3.679	122.3
H_2	2.920	26.41
N_2	3.681	67.89
CO	3.705	71.49

Table 2. Errors for several low-level direct dynamics and approximate interaction potential energy surfaces relative to counterpoise corrected QCISD(T)/CBS energies

Direct dynamics

M	PES[a]	$\varepsilon_{\mathrm{min}}$, cm^{-1}	$\varepsilon_{\mathrm{rel}}$, %	$\varepsilon_{\mathrm{rep}}$, Å
He	MP2	3.9	13.9	0.04
Ne	MP2	4.9	7.9	0.02
CH_4	MP2	10.3	5.4	0.01
H_2	MP2	24.3	23.7	0.04
	SAC	11.1	10.8	0.02

Separable pairwise

M	$V_{\mathrm{M–T}}$	$\varepsilon_{\mathrm{min}}$, cm^{-1}	$\varepsilon_{\mathrm{rel}}$, %	$\varepsilon_{\mathrm{rep}}$, Å
He	exp/6	1.1	4.0	0.04
	LJ-A	1.8	6.5	0.26
	LJ-B	7.0	25.0	0.13
Ne	exp/6	4.0	6.5	0.03
Ar	exp/6	6.8	4.9	0.03
Kr	exp/6	7.8	4.8	0.03
H_2	exp/6 RP	24.8	24.9	0.06
	exp/6 R	30.9	24.2	0.12
	exp/6 P	25.6	30.1	0.10
N_2	exp/6 RP	39.5	24.7	0.04
	exp/6 R	24.9	15.5	0.03
	exp/6 P	23.1	14.4	0.04
CO	exp/6 RP	36.3	20.5	0.12
	exp/6 R O-in	45.4	25.7	0.18
	exp/6 R C-in	35.0	19.8	0.41
	exp/6 P	68.5	38.7	0.24

[a] The aug'-cc-pVDZ basis set was used for the MP2 and SAC calculations.

Table 3. Frequencies ω and rotational constants B for CH_4 (cm^{-1})

	ω				B
experimental[a]	3019	2917	1534	1306	5.24
MP2[b]	3209	3065	1565	1344	5.19
SAC[b]	3194	3042	1545	1321	5.19
TB	3252	3162	1690	1570	5.24

[a] Ref. [25]

[b] The aug'-cc-pVDZ basis set was used for the MP2 and SAC calculations.

Table 4. Predicted energy transfer parameters for eq 1

	α_{300}, cm^{-1}	n
He	117	0.95
Ne	104	0.86
Ar	115	0.75
Kr	123	0.67
H_2	162	0.83
N_2	130	0.76
CO	130	0.76
CH_4	390	0.60

Figure Captions

Fig. 1 CH_4 + He interaction potential for face (black), edge (red), and vertex (blue) approaches. The solid lines in all four panels are QCISD(T)/CBS energies, and the dashed lines are (a) MP2/aug'-cc-pVDZ, (b) exp/6, (c) LJ-A, and (d) LJ-B energies. The insets highlight the van der Waals well.

Fig. 2 CH_4 + H_2 interaction potential for the QCISD(T)/CBS (solid) and exp/6 (dashed) methods. The color code for the approaches is the same as in Fig. 1. H_2 is aligned in the direction of the approach (radially) in (a,c,e) and perpendicularly in (b,d,f). Three exp/6 fits are shown: (a,b) the compromise (RP) fit, (c,d) the radial-only (R) fit, and (e,f) the perpendicular-only (P) fit.

Fig. 3 Average downward energy transfer for M = He for five potential energy surfaces. The symbols are results obtained from single temperature ensembles. The solid lines are results obtained using the multitemperature sampling scheme. The dashed lines connect the LJ results.

Fig. 4 Average downward energy transfer for M = Ne for several potential energy surfaces. The symbols are results obtained from single temperature ensembles. The solid lines are results obtained using the new multitemperature sampling scheme.

Fig. 5 Average downward energy transfer for M = H_2 for four potential energy surfaces.

Fig. 6 Average downward energy transfer for M = N_2 (solid) and CO (dashed) for several potential energy surfaces. The TB+exp/6 P potential was not tested for CO.

Fig. 7 Energy transfer averages scaled to Lennard-Jones collision rates for deactivating collisions in eight baths at (a) 300 and (b) 2000 K for the MP2 (open symbols) and TB+exp/6 (closed symbols) potential energy surfaces. For the diatomic baths, the average of the several TB+exp/6 parameterizations considered is shown. The error bars are 1σ statistical uncertainties, except for the TB+exp/6 results for the diatomic baths where the error bars are the standard deviations of the results for the several TB+exp/6 parameterizations.

Note that the CH_4 results are scaled down by a factor of 3 and 2 at 300 K and 2000 K, respectively.

Fig. 8 Energy transfer rate coefficients for deactivating collisions in eight baths at (a) 300 and (b) 2000 K and 1 Torr for the MP2 (open symbols) and TB+exp/6 (closed symbols) potential energy surfaces. For the diatomic baths, the average of the several TB+exp/6 parameterizations considered is shown. The error bars are 1σ statistical uncertainties, except for the TB+exp/6 results for the diatomic baths where the error bars are the standard deviations of the results for the several TB+exp/6 parameterizations. Note that the CH_4 results are scaled down by a factor of 3 and 2 at 300 K and 2000 K, respectively.

Fig. 9 (a) The average energy transferred in deactivating collisions and (b) the root-mean-squared energy transferred for eight baths. The CH_4 results are scaled down by a factor of 2.

Fig. 10 (a) The average energy transfer rate coefficient in deactivating collisions and (b) root-mean-squared energy transfer rate coefficient at 1 Torr for eight baths.

Fig. 11 A comparison of the (a) low pressure limit dissociation rate coefficient, (b) association rate coefficient at 300 K, and (c) dissociation rate coefficient at 1150 K for CH_4 in eight baths.

Fig. 12 The present predicted (a) low pressure and (b) falloff decomposition rate coefficients for CH_4 in Ar (black solid lines) compared with several experimental results in Ar and Kr (thin lines in (a) and symbols in (b)) and with the recommended value of Baulch et al. (blue dotted lines). The effect on the present prediction of scaling the vibrational frequencies to increase the density of states of CH_4 at threshold by a factor of two is shown as dashed red lines.

Fig. 13 Predicted falloff rate coefficients for CH_4 decomposition in CH_4 (black lines). Several experimental results (symbols) and the recommended values of Baulch et al. (blue dotted lines) are also shown. The effect on the present prediction of increasing the density of states of CH_4 at threshold by a factor of two is shown as dashed red lines.

Fig. 14 Association (k_a) and dissociation (k) rate coefficients for CH_4 in He at (a) 300 K, (b) 600 K, and (c) 1150 K. The present predicted values (black solid lines)

are compared with the recommended values of Baulch et al. (blue dashed lines) and experimental values from two groups[59,63] (circles). The red dotted lines show the effect on the present predicted values of artificially doubling the density of states of CH_4 at threshold. The horizontal lines show the high pressure limits.

Figure 1

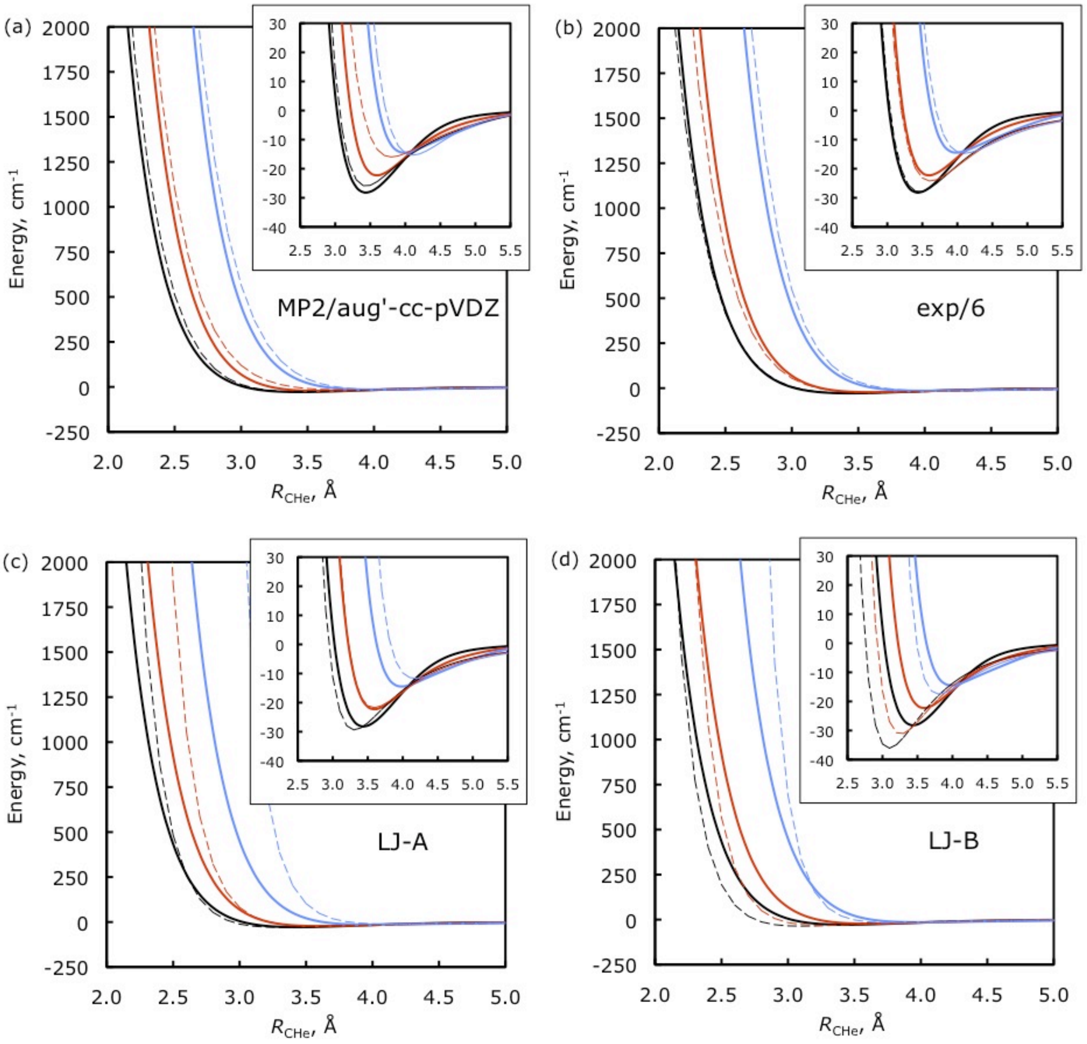

Fig. 1 CH_4 + He interaction potential for face (black), edge (red), and vertex (blue) approaches. The solid lines in all four panels are QCISD(T)/CBS energies, and the dashed lines are (a) MP2/aug'-cc-pVDZ, (b) exp/6, (c) LJ-A, and (d) LJ-B energies. The insets highlight the van der Waals well.

Figure 2

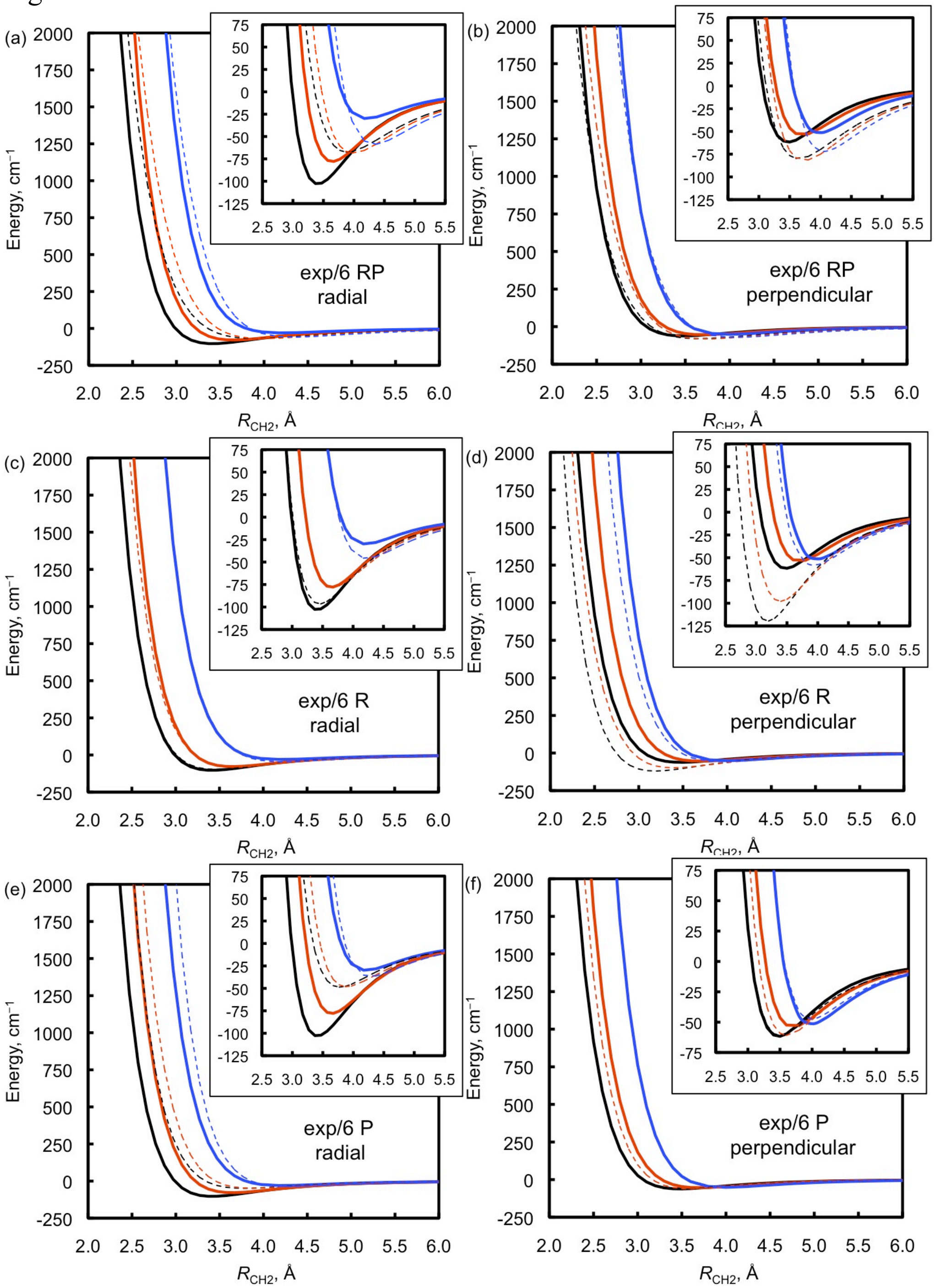

Fig. 2 $CH_4 + H_2$ interaction potential for the QCISD(T)/CBS (solid) and exp/6 (dashed) methods. The color code for the approaches is the same as in Fig. 1. H_2 is aligned in the direction of the approach (radially) in (a,c,e) and perpendicularly in (b,d,f). Three exp/6 fits are shown: (a,b) the compromise (RP) fit, (c,d) the radial-only (R) fit, and (e,f) the perpendicular-only (P) fit.

Figure 3

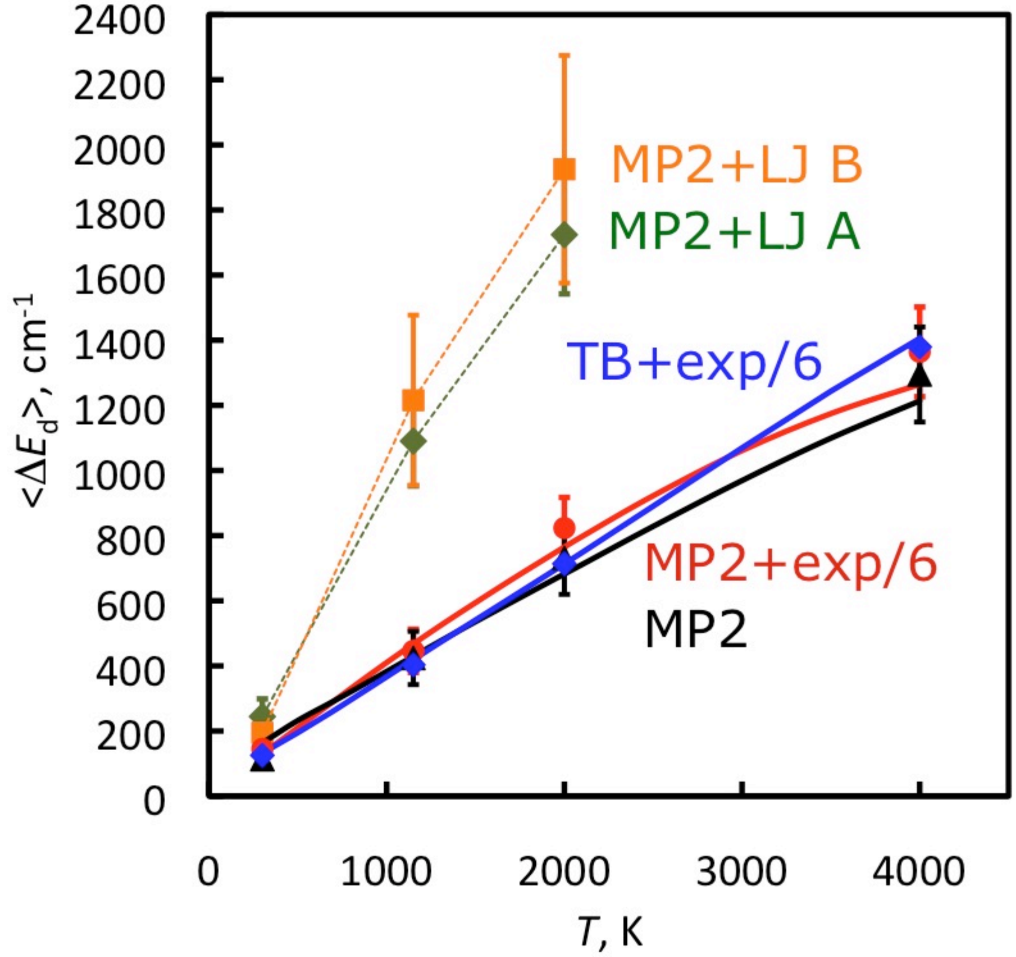

Fig. 3 Average downward energy transfer for M = He for five potential energy surfaces. The symbols are results obtained from single temperature ensembles. The solid lines are results obtained using the multitemperature sampling scheme. The dashed lines connect the LJ results.

Figure 4

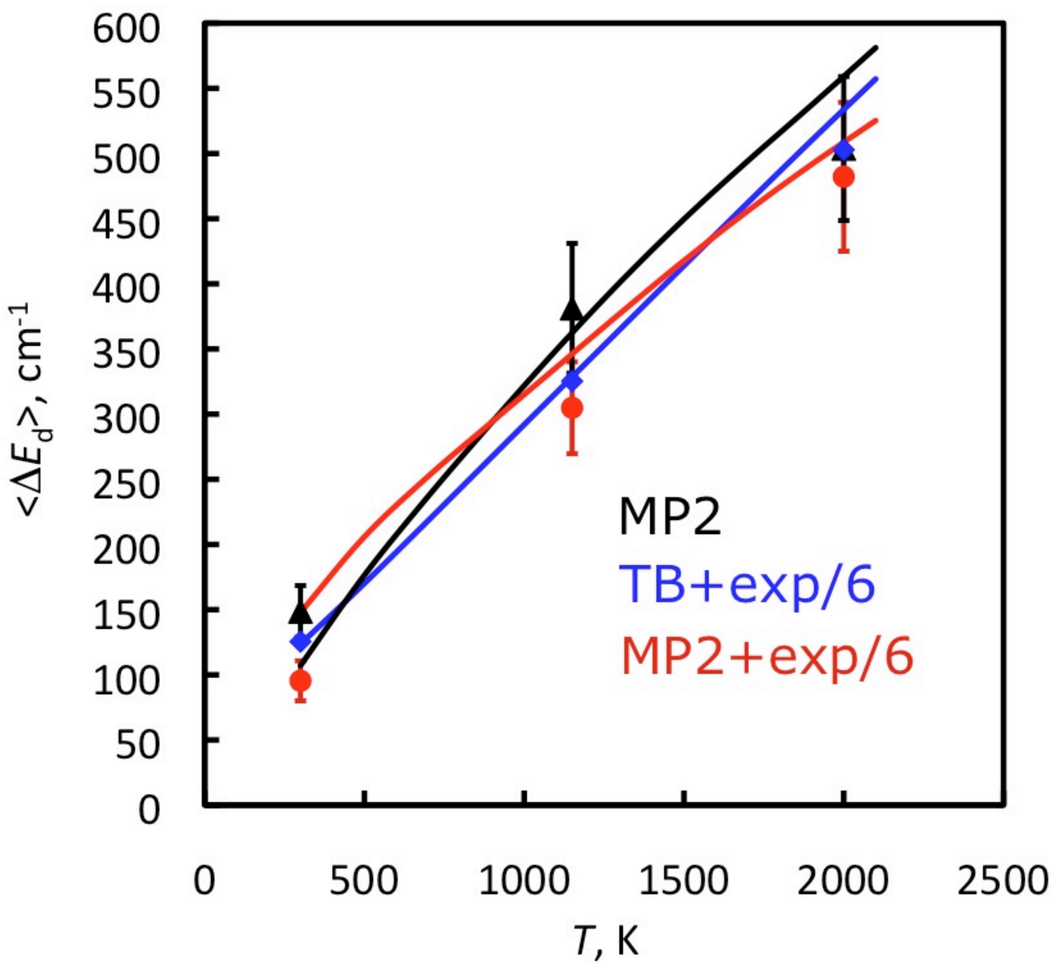

Fig. 4 Average downward energy transfer for M = Ne for several potential energy surfaces. The symbols are results obtained from single temperature ensembles. The solid lines are results obtained using the new multitemperature sampling scheme.

Figure 5

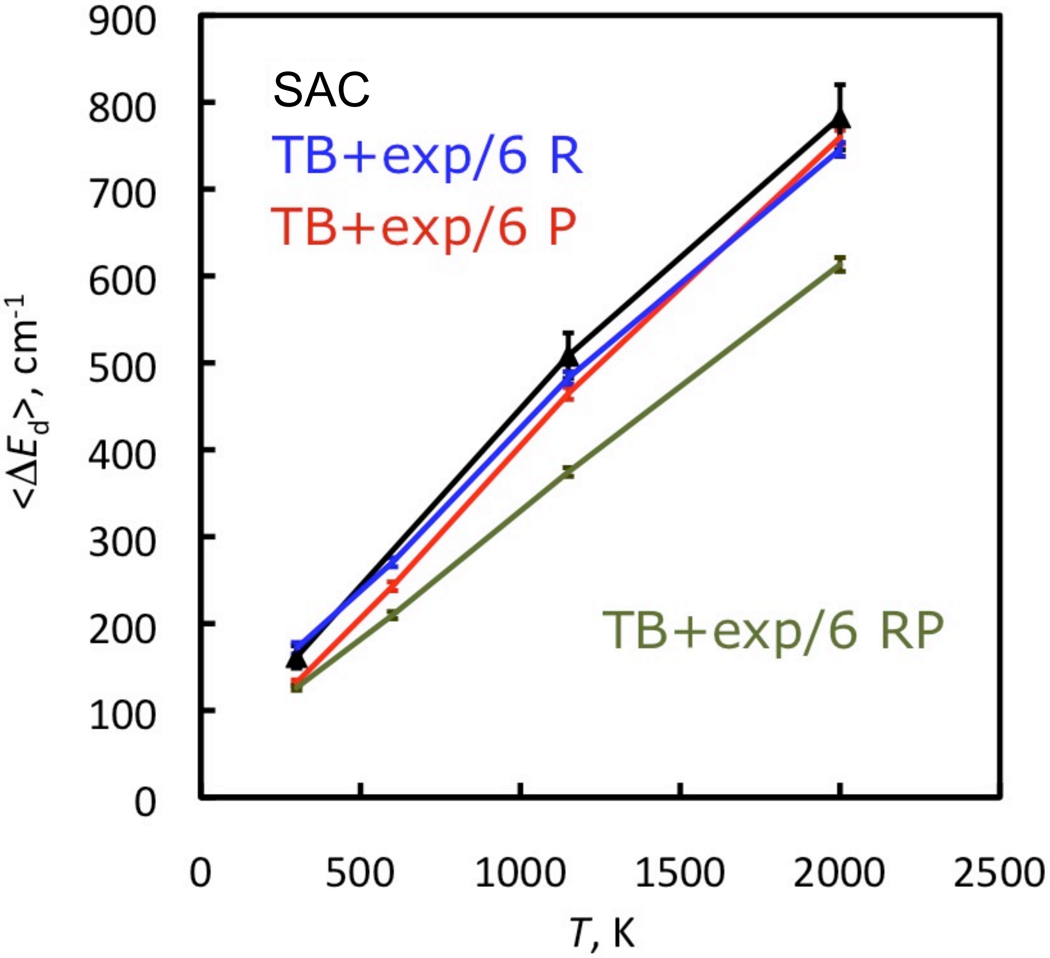

Fig. 5 Average downward energy transfer for M = H_2 for four potential energy surfaces.

Figure 6

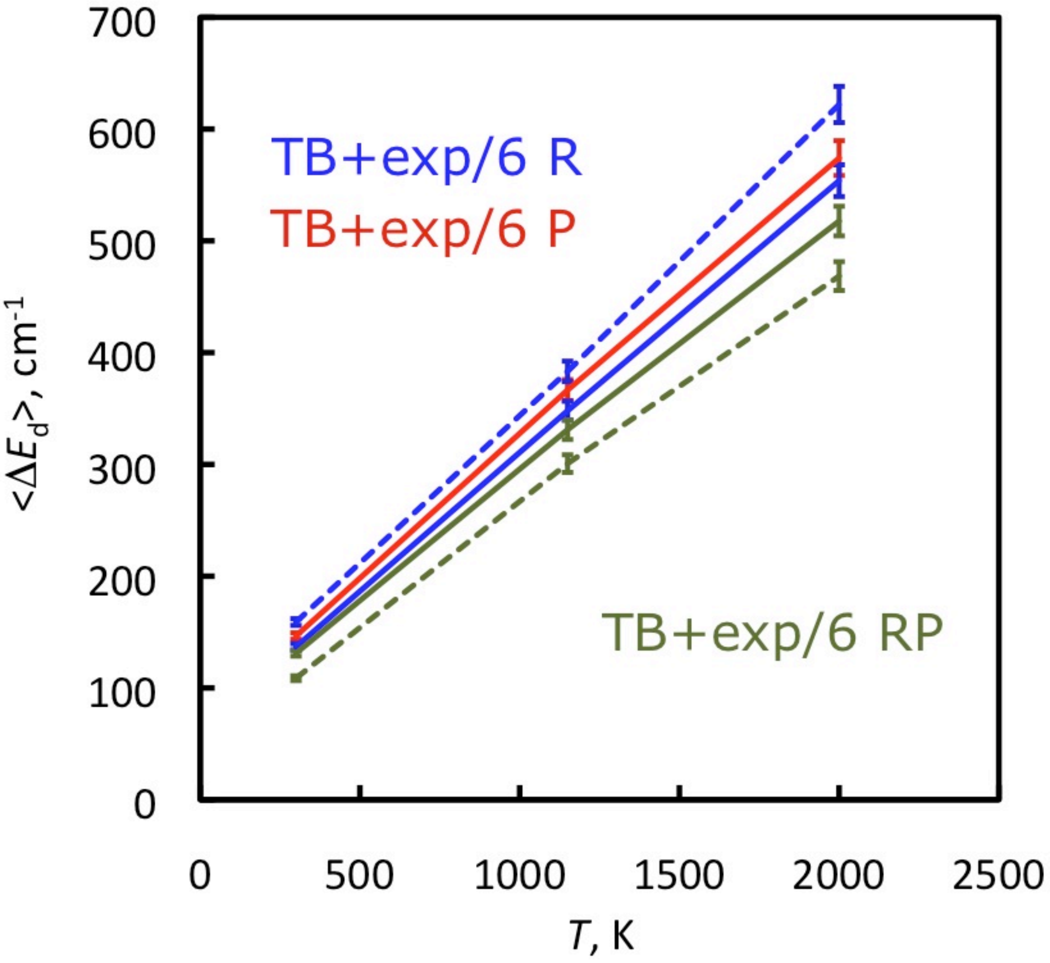

Fig. 6 Average downward energy transfer for M = N_2 (solid) and CO (dashed) for several potential energy surfaces. The TB+exp/6 P potential was not tested for CO.

Figure 7

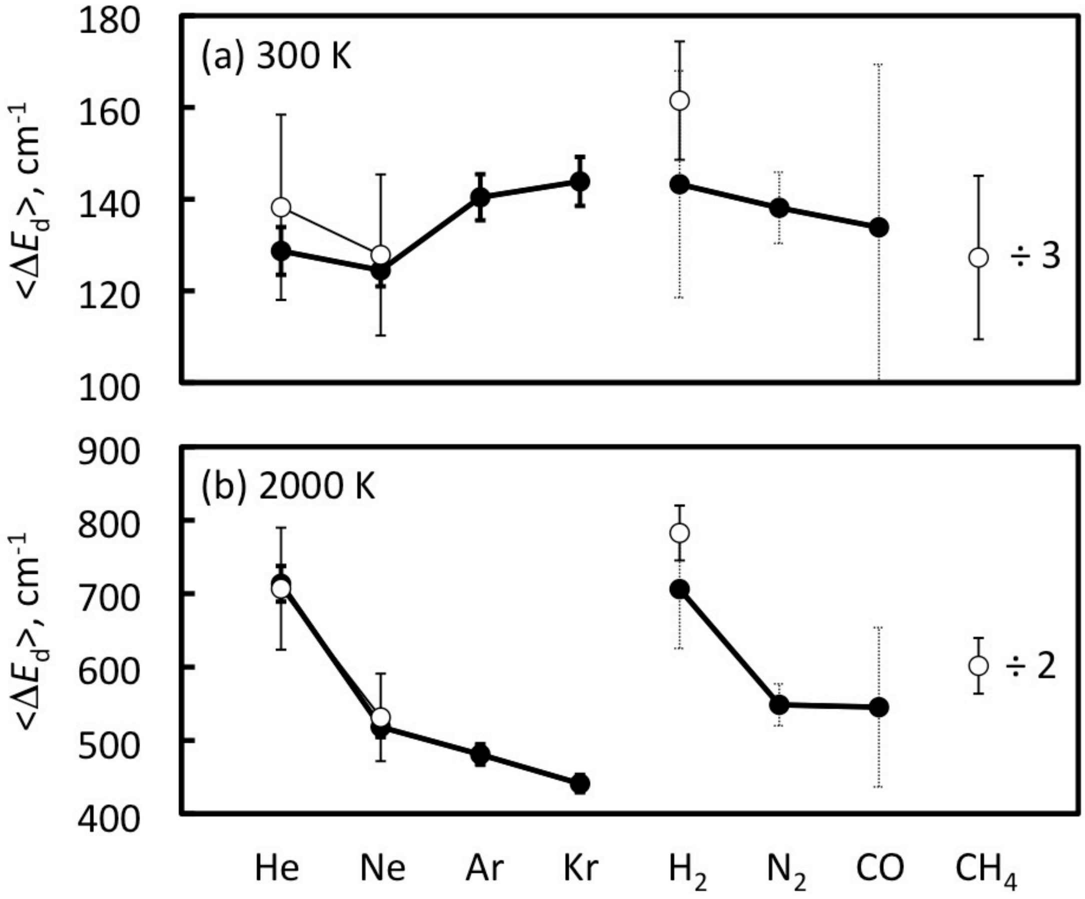

Fig. 7 Energy transfer averages scaled to Lennard-Jones collision rates for deactivating collisions in eight baths at (a) 300 and (b) 2000 K for the MP2 (open symbols) and TB+exp/6 (closed symbols) potential energy surfaces. For the diatomic baths, the average of the several TB+exp/6 parameterizations considered is shown. The error bars are 1σ statistical uncertainties, except for the TB+exp/6 results for the diatomic baths where the error bars are the standard deviations of the results for the several TB+exp/6 parameterizations. Note that the CH_4 results are scaled down by a factor of 3 and 2 at 300 K and 2000 K, respectively.

Figure 8

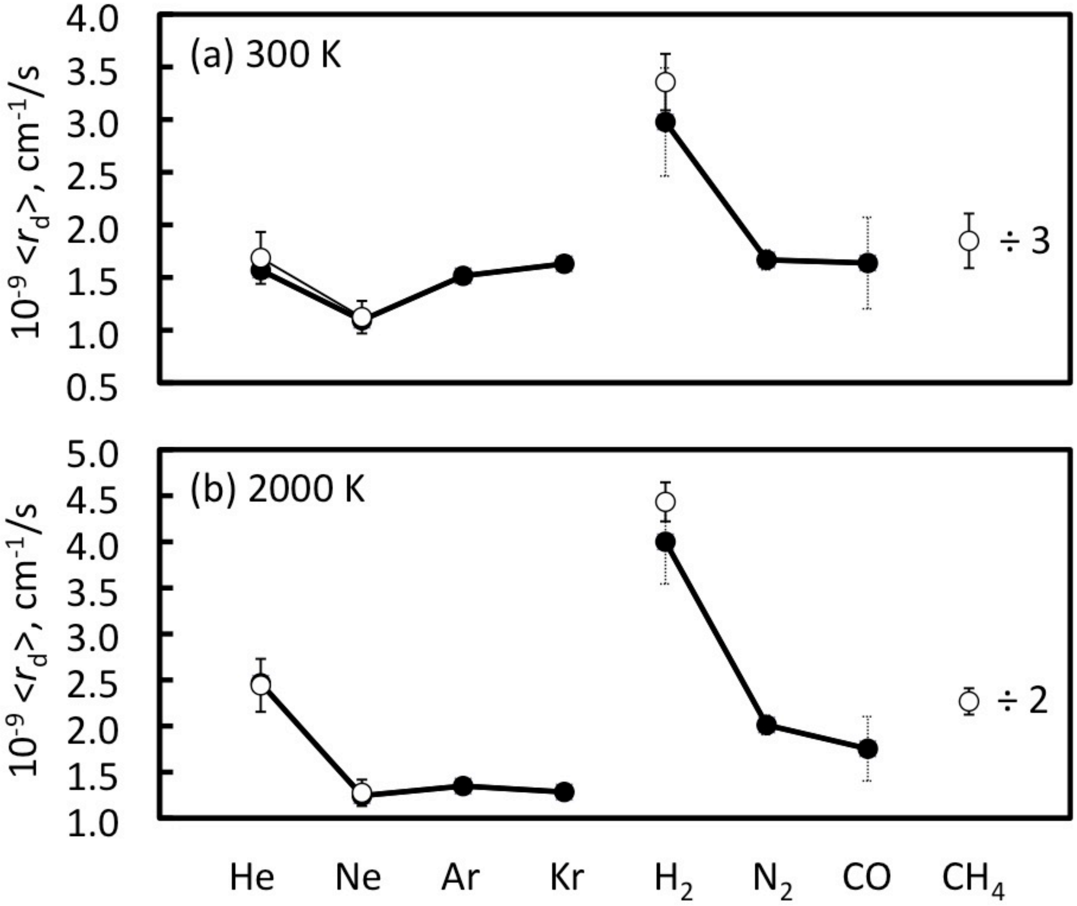

Fig. 8 Energy transfer rate coefficients for deactivating collisions in eight baths at (a) 300 and (b) 2000 K and 1 Torr for the MP2 (open symbols) and TB+exp/6 (closed symbols) potential energy surfaces. For the diatomic baths, the average of the several TB+exp/6 parameterizations considered is shown. The error bars are 1σ statistical uncertainties, except for the TB+exp/6 results for the diatomic baths where the error bars are the standard deviations of the results for the several TB+exp/6 parameterizations. Note that the CH_4 results are scaled down by a factor of 3 and 2 at 300 K and 2000 K, respectively.

Figure 9

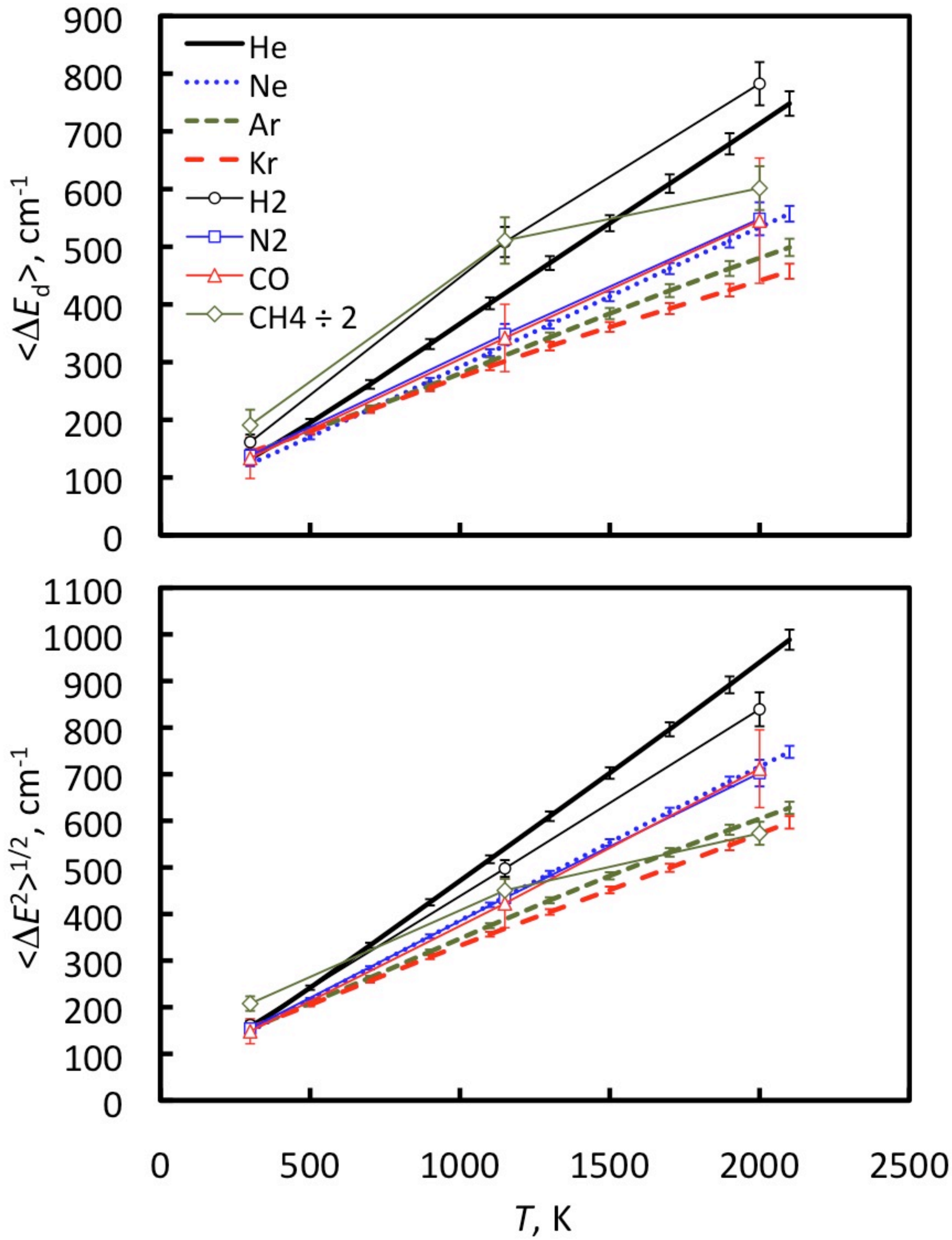

Fig. 9 (a) The average energy transferred in deactivating collisions and (b) the root-mean-squared energy transferred for eight baths. The CH_4 results are scaled down by a factor of 2.

Figure 10

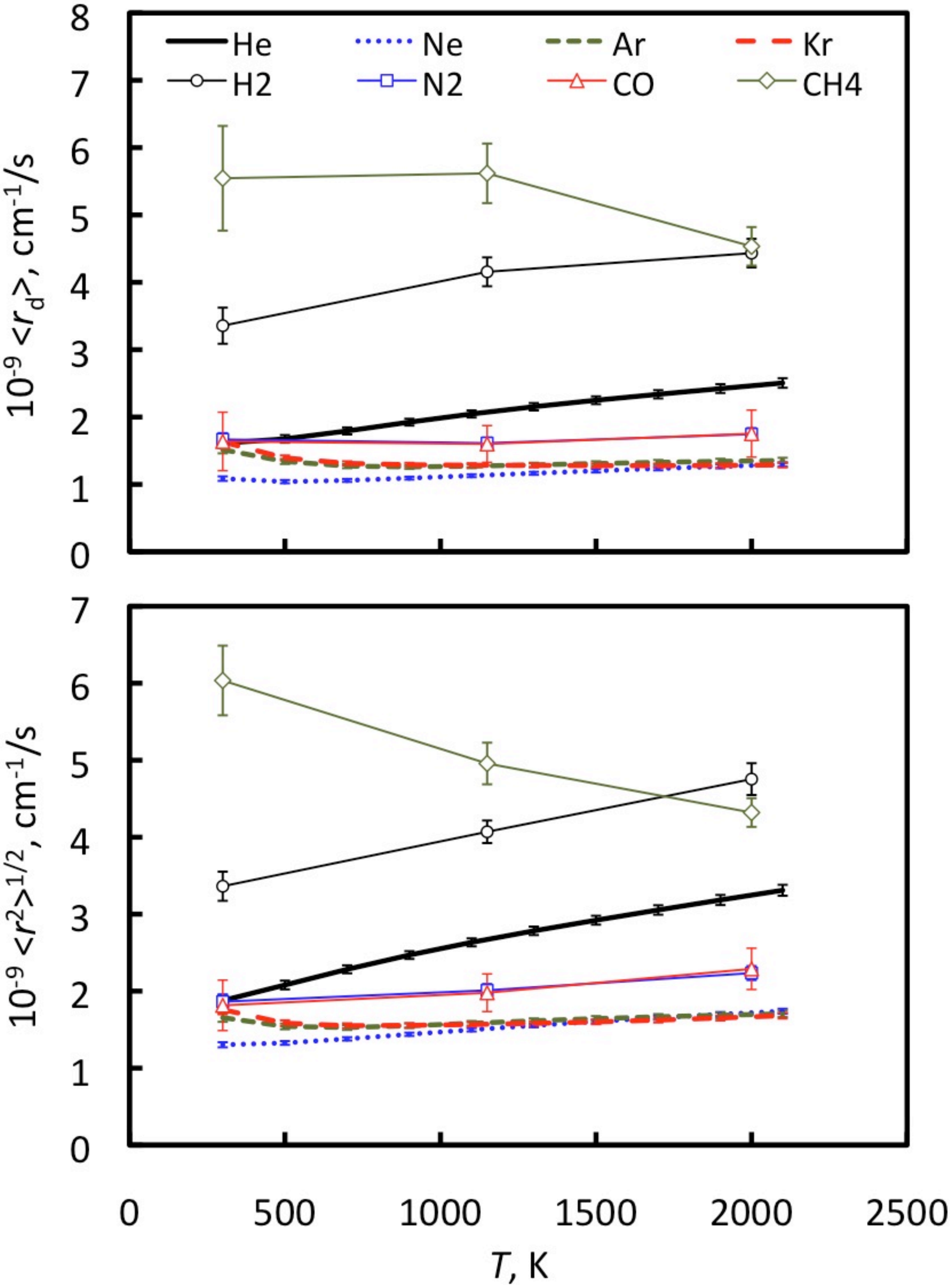

Fig. 10 (a) The average energy transfer rate coefficient in deactivating collisions and (b) root-mean-squared energy transfer rate coefficient at 1 Torr for eight baths.

Figure 11

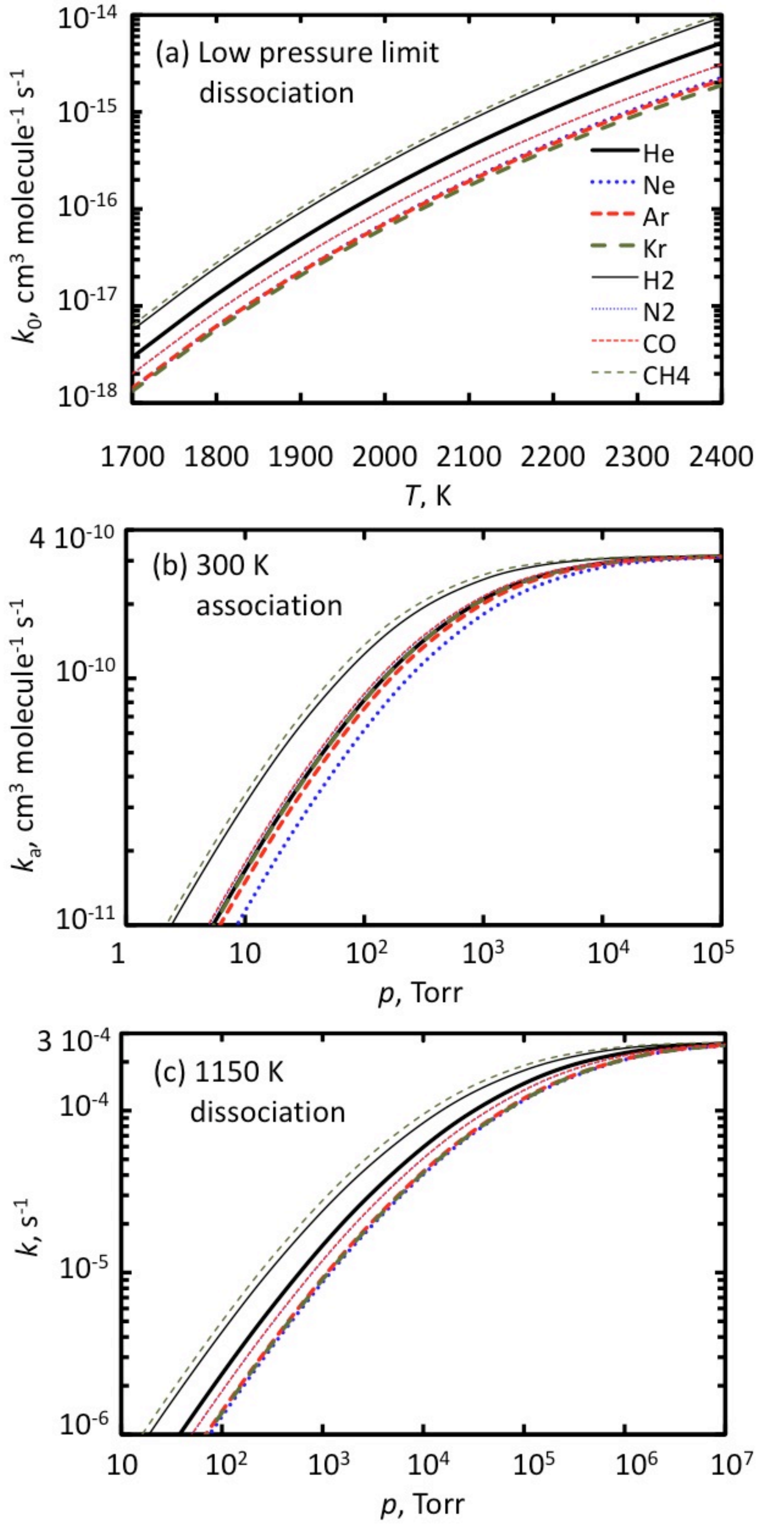

Fig. 11 A comparison of the (a) low pressure limit dissociation rate coefficient, (b) association rate coefficient at 300 K, and (c) dissociation rate coefficient at 1150 K for CH_4 in eight baths.

Figure 12

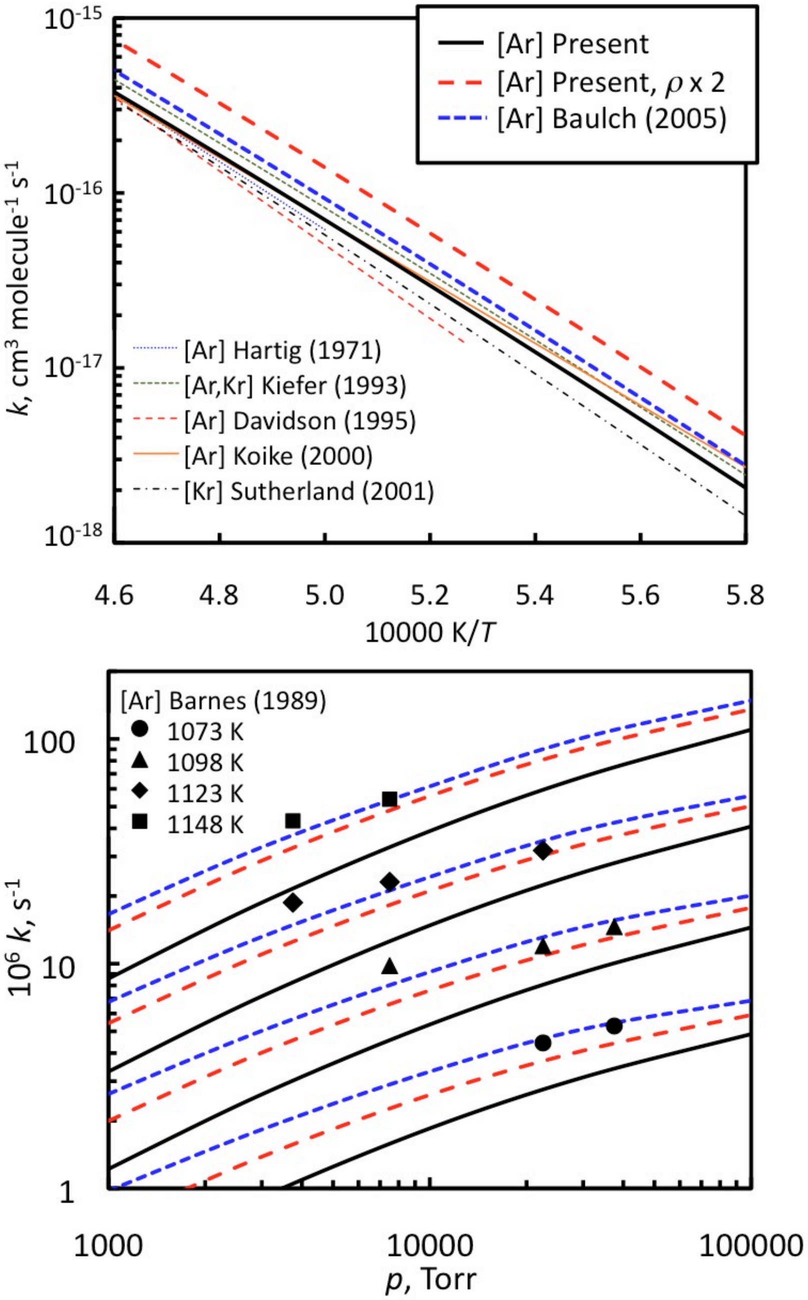

Fig. 12 The present predicted (a) low pressure and (b) falloff decomposition rate coefficients for CH_4 in Ar (black solid lines) compared with several experimental results in Ar and Kr (thin lines in (a) and symbols in (b)) and with the recommended value of Baulch et al. (blue dotted lines). The effect on the present prediction of scaling the vibrational frequencies to increase the density of states of CH_4 at threshold by a factor of two is shown as dashed red lines.

Figure 13

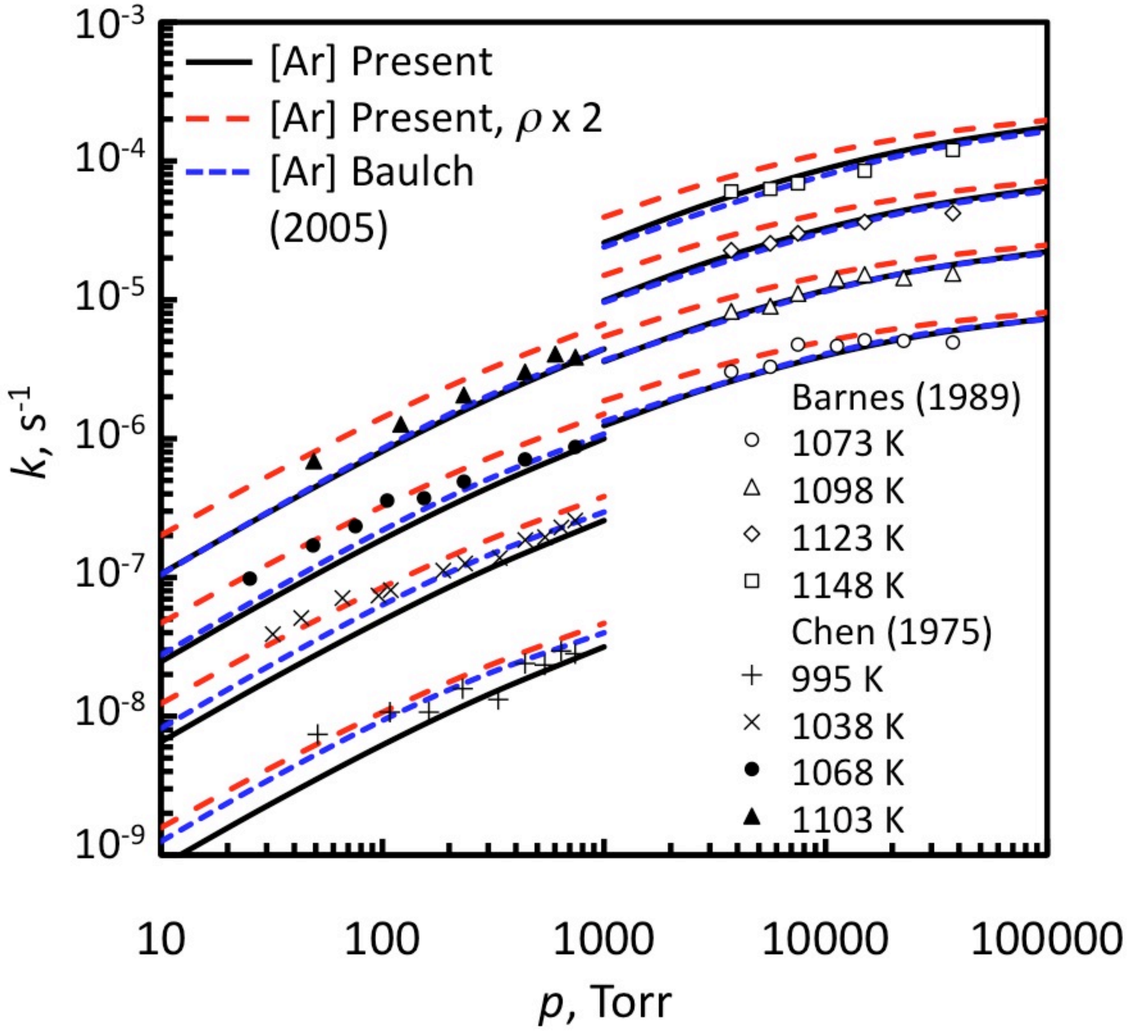

Fig. 13 Predicted falloff rate coefficients for CH_4 decomposition in CH_4 (black lines). Several experimental results (symbols) and the recommended values of Baulch et al. (blue dotted lines) are also shown. The effect on the present prediction of increasing the density of states of CH_4 at threshold by a factor of two is shown as dashed red lines.

Figure 14

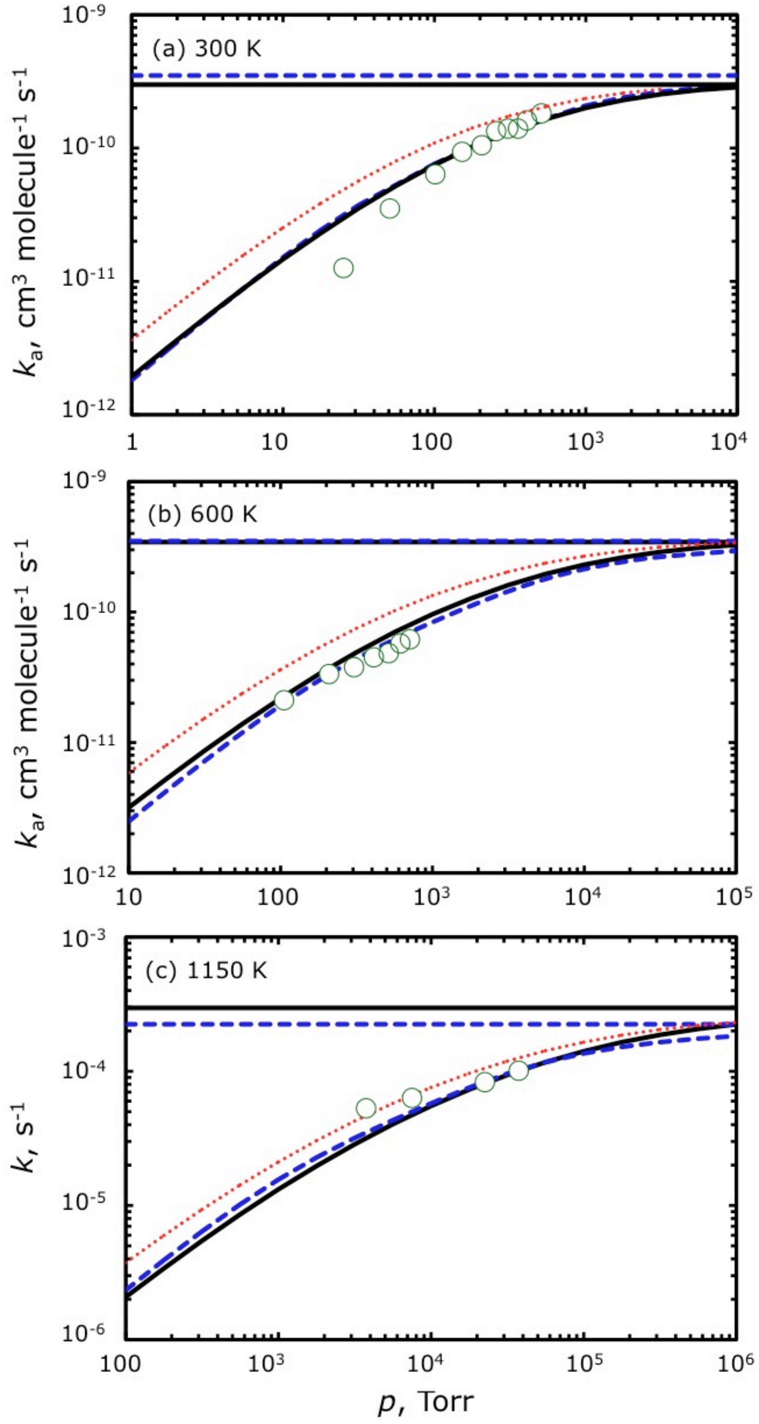

Fig. 14 Association (k_a) and dissociation (k) rate coefficients for CH_4 in He at (a) 300 K, (b) 600 K, and (c) 1150 K. The present predicted values (black solid lines) are compared with the recommended values of Baulch et al. (blue dashed lines) and experimental values from two groups[59,63] (circles). The red dotted lines show the effect on the present predicted values of artificially doubling the density of states of CH_4 at threshold. The horizontal lines show the high pressure limits.

References

---

[1] Troe, J. *J. Chem. Phys.* **1977**, *66*, 4745, 4758.

[2] Barker, J. R.; Golden, D. M. *Chem. Rev.* **2003**, *103*, 4577.

[3] Pilling, M. J.; Robertson, S. H. *Annu. Rev. Phys. Chem.* **2003**, *54*, 245.

[4] Miller, J. A.; Klippenstein, S. J. *J. Phys. Chem. A* **2006**, *110*, 10528.

[5] Fernandez-Ramos, A.; Miller, J. A.; Klippenstein, S. J.; Truhlar, D. G. *Chem. Rev.* **2006**, *106*, 4518.

[6] Smith, S. C.; Gilbert, R. G. *Int. J. Chem. Kinet.* **1988**, *20*, 307.

[7] Miller, J. A.; Klippenstein, S. J.; Raffy, C. *J. Phys. Chem. A* **2002**, *106*, 4904.

[8] Brown, N. J.; Miller, J. A *J. Chem. Phys.* **1984**, *80*, 5568.

[9] Gelb, A. *J. Phys. Chem.* **1985**, *89*, 4189.

[10] Jasper, A. W.; Miller, J. A. *J. Phys. Chem. A* **2009**, *113*, 5612.

[11] Barker, J. R.; Weston, R. E. *J. Phys. Chem. A*, **2010**, *114*, 10619.

[12] Bruehl, M.; Schatz, G. C. *J. Phys. Chem.* **1988**, *92*, 7223.

[13] Lendvay, G.; Schatz, G. C. *J. Phys. Chem.* **1991**, *95*, 8748.

[14] Lenzer, T.; Luther, K.; Troe, J; Gilbert, R. G.; Lim, K. F. *J. Chem. Phys.* **1995**, *103*, 626.

[15] Golden, D. M. *Int. J. Chem. Kinet.* **2008**, *41*, 245.

[16] Sellevåg, S. R.; Georgievskii, Y.; Miller, J. A. *J. Phys. Chem. A* **2008**, *112*, 5095.

[17] Kiefer, J. H.; Santhanam, S.; Srinivasan, N. K.; Tranter, R. S.; Klippenstein, S. J.; Oehlschlaeger, M. A. *Proc. Combust. Inst.* **2005**, *30*, 1129.

[18] Yang, X.; Jasper, A. W., Kiefer, J. H.; Tranter, R. S. *J. Phys. Chem. A* **2009**, *113*, 8318.

[19] Gibert, R. G. *Int. Rev. Phys. Chem.* **1991**, *10*, 319.

[20] Clarke, D. L.; Oref, I.; Gilbert, R. G.; Lim, K. F. *J. Chem. Phys.* **1992**, *96*, 5983.

[21] Linhananta, A.; Lim, K. F. *Phys. Chem. Chem. Phys.* **2000**, *2*, 1385.

[22] Yerram, M. L.; Brenner, J. D.; King, K. D.; Barker, J. R. *J. Phys. Chem.* **1990**, *94*, 6341.

[23] Michael, J. V.; Su, M.-C.; Sutherland, J. W.; Carroll, J. J.; Wagner, A. F. *J. Phys. Chem. A* **2002**, *106*, 5297.

[24] Harding, L. B.; Georgievskii, Y.; Klippenstein, S. J. *J. Phys. Chem. A* **2005**, *109*, 4646.

---

[25] NIST Chemistry WebBook, NIST Standard Reference Database Number 69, Eds. P.J. Linstrom and W.G. Mallard, National Institute of Standards and Technology, Gaithersburg MD, 20899, http://webbook.nist.gov.

[26] Medvedev, D. M.; Harding, L. B.; Gray, S. K. *Mol. Phys.* **2006**, *104*, 73.

[27] Hirschfelder, J. O.; Curtiss, C. F.; Bird, R. B. *Molecular Theory of Gases and Liquids* (Wiley, New York, 1954), pp. 1110, 1212.

[28] VariFlex, version 2.0, Klippenstein, S. J.; Wagner, A. F.; Dunbar, R. C.; Wardlaw, D. M.; Robertson, S. H.; Miller, J. A., Argonne National Laboratory, 2006.

[29] Gordon, M. S.; Truhlar, D. G. *J. Am. Chem. Soc.* **1986**, *108*, 5412.

[30] Zhao, Y.; Truhlar, D. G. *Acc. Chem. Res.* **2008**, *41*, 157.

[31] Alexander; W. A.; Troya, D. *J. Phys. Chem.* **2006**, *110*, 10834.

[32] Allen, M. P.; Tildesley, D. J. *Computer Simulation of Liquids* (Oxford University Press, New York, 1992), p. 21.

[33] Hack, M. D.; Truhlar, D. G. *J. Chem. Phys.* **1999**, *110*, 4315 fit the data of Kołos, W.; Wolniewicz, L. J. Chem. Phys. **1965**, *43*, 2429.

[34] Le Roy, R. J.; Huang, Y.; Jary, C. *J. Chem. Phys.* **2006**, *125*, 164310.

[35] Krupenie, P.; Weissman, S. *J. Chem. Phys.* **1965**, *43*, 1529.

[36] Hoffmann, R. *J. Chem. Phys.* **1963**, *39*, 1397; **1964**, *40*, 2047, 2474, 2480, 2745.

[37] Slater, J. C.; Koster, G. F. *Phys. Rev.* **1954**, *94*, 1498.

[38] Wang, Y.; Mak, C. H. *Chem. Phys. Lett.* **1995**, *235*, 37.

[39] TB, version 1.0.1, Liu, T.; Truhlar, D. G., University of Minnesota, 2004. See comp.chem.umn.edu/tbpac. T. Liu, PhD Thesis, University of Minnesota, 2000.

[40] Andersen, H. C. *J. Chem. Phys.* **1980**, *72*, 2348.

[41] Faist, M. B.; Muckerman, J. T.; Schubert, F. E. *J. Chem. Phys.* **1978**, *69*, 4087.

[42] Efron, B. *Ann. Stat.* **1979**, *7*, 1.

[43] Nangia, S.; Jasper, A. W.; Miller, III, T. F.; Truhlar, D. G. *J. Chem. Phys.* **2004**, *120*, 3586.

[44] Lim, K. F.; Gilbert, R. G. *J. Phys. Chem.* **1990**, *94*, 72, 77.

[45] DiNT, Version 1.0, Jasper, A. W.; Oana, C. M.; Truhlar, D. G., Sandia National Laboratories and University of Minnesota, 2010. See www.sandia.gov/~ajasper/dint.

---

[46] MOLPRO, Version 2006.1, Werner, H.-J.; Knowles, P. J.; Lindh, R.; Manby, F. R.; Schütz, M.; Celani, P.; Korona, T.; Rauhut, G.; Amos, R. D.; Bernhardsson, A.; Berning, A.; Cooper, D. L.; Deegan, M. J. O.; Dobbyn, A. J.; Eckert, F.; Hampel, C.; Hetzer, G.; Lloyd, A. W.; McNicholas, S. J.; Meyer, W.; Mura, M. E.; Nicklaß, A.; Palmieri, P.; Pitzer, R.; Schumann, U.; Stoll, H.; Stone A. J.; Tarroni, R.; T. Thorsteinsson. See www.molpro.net.

[47] Lenzer, T.; Luther, K. *J. Chem. Phys.* **1996**, *105*, 10944.

[48] Meroueh, O.; Hase, W. L. *J. Phys. Chem. A* **1999**, *103*, 3981.

[49] Brunsvold, A. L.; Garton, D. J.; Minton, T. K.; Troya, D.; Schatz, G. C; *J. Chem. Phys.* **2004**, *121*, 11702.

[50] Ahumada, J. J.; Michael, J. V.; Osborne, D. T. *J. Chem. Phys.* **1972**, *57*, 3736.

[51] Michael, J. V.; Osborne, D. T.; Suess, G. N. *J. Chem. Phys.* **1972**, *58*, 2800.

[52] Michael, J. V.; Payne, W. A.; Whytock, D. A. *J. Chem. Phys.* **1976**, *65*, 4830. Whytock, A. D.; Michael, J. V.; Payne, W. A. *Chem. Phys. Lett.* **1976**, *42*, 466.

[53] Hartig, R.; Troe, J.; Wagner, H. G. *Symp. Int. Combust. Proc.* **1971**, *13*, 147.

[54] Davidson, D. F.; DiRosa, M. D.; Chang, A. Y.; Hanson, R. K.; Bowman, C. T. *Symp. Int. Combust. Proc.* **1992**, *24*, 589. Davidson, D. F.; Hanson, R. K.; Bowman, C. T. *Int. J. Chem. Kinet.* **1995**, *27*, 305.

[55] Kiefer, J. H.; Kumaran, S. S. *J. Phys. Chem.* **1993**, *97*, 414.

[56] Koike, T.; Kudo, M.; Yamada, H. *Int. J. Chem. Kinet.* **2000**, *32*, 1.

[57] Sutherland, J. W.; Su, M.-C.; Michael, J. V. *Int. J. Chem. Kinet.* **2001**, *33*, 669.

[58] Baulch, D. L.; Bowman, C. T.; Cobos, C. J.; Cox, R. A.; Just, Th.; Kerr, J. A.; Pilling, M. J.; Stocker, D.; Troe, J.; Tsang, W.; Walker, R. W.; Warnatz, *J. Phys. Chem. Ref. Data* **2005**, *34*, 757.

[59] Barnes, R. W.; Pratt, G. L.; Wood, S. W. *J. Chem. Soc. Faraday Trans. 2* **1989**, *85*, 229.

[60] Nguyen, T. L.; Barker, J. R. *J. Phys. Chem. A* **2010**, *114*, 3718.

[61] Schmatz, S. *Chem. Phys.* **2008**, *346*, 198.

[62] Chen, C. J.; Back, M. H.; Back, A. R. *Can. J. Chem.* **1975**, *53*, 3580.

---

[63] Brouard, M.; Macpherson, M. T.; Pilling, M. J.; Tulloch, J. M.; Williamson, A. P. *Chem. Phys. Lett.* **1985**, *113*, 413. Brouard, M.; Macpherson, M. T.; Pilling, *J. Phys. Chem.* **1989**, *93*, 4047.

[64] Troe, J.; Ushankov, V. G. *J. Phys. Chem. A* **2009**, *113*, 3940.